



## Volumetric distribution of perivascular space in relation to mild cognitive impairment



Farshid Sepehrband<sup>a,b,\*</sup>, Giuseppe Barisano<sup>a,c</sup>, Nasim Sheikh-Bahaei<sup>d,e</sup>,  
Jeiran Choupan<sup>a,f</sup>, Ryan P. Cabeen<sup>a</sup>, Kirsten M. Lynch<sup>a</sup>, Malcolm S. Crawford<sup>a,g</sup>,  
Haoyu Lan<sup>a</sup>, Wendy J. Mack<sup>h</sup>, Helena C. Chui<sup>b,e</sup>, John M. Ringman<sup>b,e</sup>,  
Arthur W. Toga<sup>a,b</sup>, for the Alzheimer's Disease Neuroimaging Initiative

<sup>a</sup>Laboratory of NeuroImaging, USC Stevens Neuroimaging and Informatics Institute, Keck School of Medicine, University of Southern California, Los Angeles, CA, USA

<sup>b</sup>Alzheimer's Disease Research Center, Keck School of Medicine, University of Southern California, Los Angeles, CA, USA

<sup>c</sup>Neuroscience Graduate Program, University of Southern California, Los Angeles, CA, USA

<sup>d</sup>Department of Radiology, Keck School of Medicine, University of Southern California, Los Angeles, CA, USA

<sup>e</sup>Department of Neurology, Keck School of Medicine, University of Southern California, Los Angeles, CA, USA

<sup>f</sup>Department of Psychology, University of Southern California, Los Angeles, CA, USA

<sup>g</sup>School of Medicine, University of California, Irvine, Irvine, CA, USA

<sup>h</sup>Department of Preventive Medicine, Keck School of Medicine, University of Southern California, Los Angeles, CA, USA

### ARTICLE INFO

#### Article history:

Received 21 April 2020

Received in revised form 25 November 2020

Accepted 8 December 2020

Available online 16 December 2020

#### Keywords:

Perivascular space  
Cognitive decline  
Alzheimer's disease  
Clearance system

### ABSTRACT

Vascular contributions to early cognitive decline are increasingly recognized, prompting further investigation into the nature of related changes in perivascular spaces (PVS). Using magnetic resonance imaging, we show that, compared to a cognitively normal sample, individuals with early cognitive dysfunction have altered PVS presence and distribution, irrespective of Amyloid- $\beta$ . Surprisingly, we noted lower PVS presence in the anterosuperior medial temporal lobe (asMTL) (1.29 times lower PVS volume fraction in cognitively impaired individuals,  $p < 0.0001$ ), which was associated with entorhinal neurofibrillary tau tangle deposition (beta (standard error) =  $-0.98$  (0.4);  $p = 0.014$ ), one of the hallmarks of early Alzheimer's disease pathology. We also observed higher PVS volume fraction in centrum semi-ovale of the white matter, but only in female participants (1.47 times higher PVS volume fraction in cognitively impaired individuals,  $p = 0.0011$ ). We also observed PVS changes in participants with history of hypertension (higher in the white matter and lower in the asMTL). Our results suggest that anatomically specific alteration of the PVS is an early neuroimaging feature of cognitive impairment in aging adults, which is differentially manifested in female.

© 2020 Elsevier Inc. All rights reserved.

### Introduction

Perivascular spaces (PVS), which are the fluid-filled area surrounding the cerebral vessels, are the major component of the brain clearance system (Wardlaw et al., 2020a,b). PVSs accommodate the flux of the cerebrospinal fluid (CSF) in the brain and are considered to play a role in brain metabolic homeostasis. Previous studies in animals suggest that the glymphatic (glia-lymphatic) system, whose main pathway is represented by the PVS, is a substantial factor in the net clearance of amyloid beta (A $\beta$ ) (Da Mesquita et al.,

2018; Iliff et al., 2012; Louveau et al., 2018; Xu et al., 2015); reduction of efflux of interstitial fluid to the CSF in PVS could lessen A $\beta$  clearance (Park et al., 2017; Rasmussen et al., 2018; Sweeney et al., 2018). Such an impaired clearance from the brain parenchyma could in part explain the accumulation of A $\beta$  (Rasmussen et al., 2018).

A $\beta$  deposition in the wall of leptomeningeal and intraparenchymal cerebral arteries is a common observation in Alzheimer's disease (AD), which is thought to be associated with the enlargement of PVS as routes of A $\beta$  clearance (Blair et al., 2015; Kalaria and Ballard, 1999; Weller et al., 2008b). PVS changes have been linked to vascular diseases, including cerebral small vessel disease, cerebral amyloid angiopathy, blood-brain barrier (BBB) breakdown, hypertension, and lacunar stroke (Charidimou et al.,

\* Corresponding author at: USC Stevens Neuroimaging and Informatics Institute, Keck School of Medicine, University of Southern California, 2025 Zonal Avenue, Los Angeles, CA 90033, USA. Tel.: 323 442-0148; fax: 323 442 0137.

E-mail address: [Farshid.sepehrband@loni.usc.edu](mailto:Farshid.sepehrband@loni.usc.edu) (F. Sepehrband).

2013; Doubal et al., 2010; Klarenbeek et al., 2013; Montagne et al., 2018; Potter et al., 2015; Rouhl et al., 2008; Wardlaw et al., 2020a,b; Weller et al., 2008a; Zhu et al., 2010b). Furthermore, an emerging body of evidence suggests that vascular changes are linked to both clearance system dysfunction (Bakker et al., 2016; Carare et al., 2008; Diem et al., 2017; Iliff and Nedergaard, 2013; Marchi et al., 2016; Nedergaard, 2013) and vasculotoxic effects of A $\beta$  and tau (Blair et al., 2015; Thomas et al., 1996).

Magnetic resonance imaging (MRI) studies have found significantly larger PVS in AD patients compared with controls in the centrum semi-ovale of the white matter (CSO-WM), but not in the basal ganglia (Banerjee et al., 2017; Ramirez et al., 2015). Interestingly, Banerjee et al. (2017) found that the PVSs in the white matter were associated with AD independently of the amyloid burden. With regards to cognition the literature is inconsistent (Francis et al., 2019; Hilal et al., 2018). Several studies suggested that increased PVS was associated with cognitive impairment (Ferguson et al., 2003; Jiménez-Balado et al., 2018; MacLulich et al., 2004; Passiak et al., 2019). Another study found no association between the number of visible PVS in the basal ganglia and cognitive impairment (Jeong et al., 2015). A recent study indicated an association of PVS in white matter with cognitive impairment (Beak et al., 2015). Two other recent studies also showed that increased PVS is associated with cognitive impairment (Chen et al., 2011; Francis et al., 2019; Ramirez et al., 2015) or lower memory performance (Valdés Hernández et al., 2020).

Early studies have mainly focused on the global PVS volume or count across the CSO-WM or basal ganglia. The anatomical distribution of PVS alterations in white matter regions, however, remains largely unexplored. To date, it has not been demonstrated whether PVS may represent an early feature of cognitive decline, nor have relationships of PVS with other pathological markers of AD, including A $\beta$  and tau been reported. To examine whether and to what extent PVS is altered in early cognitive decline, we performed a comprehensive data-driven analysis of the multi-modal data of the Alzheimer's Disease Neuroimaging Initiative 3 (ADNI-3) participants ( $N = 596$ ). Because A $\beta$  and tau can both lead to cerebral blood vessel abnormalities (Bennett et al., 2018; Iadecola, 2017; Kisler et al., 2017), we mapped PVS using MRI data and analyzed the relationship between PVS volume fraction and A $\beta$  and tau accumulation as measured in positron emission tomography (PET) images. Additionally, we investigated whether PVS distribution and appearance on MRI are influenced by the *APOE* gene, whose  $\epsilon 4$  variant represents one of the strongest genetic risk factors for AD (Corder et al., 1993).

## 2. Methods

### 2.1. Study participants

Data used in the preparation of this article were obtained from the ADNI-3 database (<http://adni.loni.usc.edu>). Data from ADNI-3 cohort (Weiner et al., 2017) were used, in which both T1-weighted (T1w) and fluid-attenuated inversion recovery (FLAIR) structural MRI were available at the time of this study. T1w and FLAIR images for 685 participants were downloaded from the ADNI database (<http://adni.loni.usc.edu>) (Toga and Crawford, 2010). Demographic information, clinical and cognitive assessment, PET, cardiovascular-related health measures, and CSF biomarkers were collected. Fifty-one participants who met the AD categorization criteria were excluded (as described in Section 2.3). An additional 37 participants who failed MRI quality control were excluded (as described in Section 2.11), resulting in a total of 596 participants.

### 2.2. Inclusion/exclusion criteria

Participants were excluded if they had any significant neurologic disease other than suspected incipient AD; exclusionary neurologic conditions included Parkinson's disease, multi-infarct dementia, Huntington's disease, normal pressure hydrocephalus, brain tumor, progressive supranuclear palsy, seizure disorder, subdural hematoma, multiple sclerosis, or history of significant head trauma followed by persistent neurologic deficits or known structural brain abnormalities. Additional and detailed inclusion and exclusion criteria are described in the ADNI-3 protocol (Weiner et al., 2017) and also copied in [Supplementary File 1](#).

### 2.3. Clinical and cognitive assessments

The ADNI clinical dataset comprises clinical information about each participant including recruitment, demographics, physical examinations, and cognitive assessment data. Demographic information including age, sex, and the years of education were gathered, which were used as covariates in all statistical analyses. A clinical interview and a general physical examination were conducted. In addition, respiration rate, blood glucose level (after overnight fasting), and systolic and diastolic pressures were acquired in the 30-day interval of the imaging visit. The cognitive assessment was performed in accordance with published standardization procedures, including standardized interview and assessment with the participant and a knowledgeable informant.

#### 2.3.1. Clinical dementia rating

Six categories of cognitive functioning (memory, orientation, judgment and problem solving, community affairs, home and hobbies, and personal care) were assessed, in which the clinical dementia rating (CDR) describes 5 degrees of impairment (Hughes et al., 1982; Morris, 1993). Participant CDR scores were obtained through a standardized interview and assessment with the participant and a knowledgeable informant.

#### 2.3.2. Mini-Mental State Examination

The Mini-Mental State Examination (MMSE) scale evaluates orientation, memory, attention, concentration, naming, repetition, comprehension, and ability to create a sentence and to copy 2 overlapping pentagons (Folstein et al., 1983). Participant MMSE scores were obtained through standardized interview and assessment with the participant and a knowledgeable informant.

Participant categorization is detailed in the ADNI-3 protocol document. In brief:

#### 2.3.3. Cognitively normal

Participants were considered cognitively normal (CN) if they had normal memory function, which was assessed using education-adjusted cutoffs on the Logical Memory II subscale from the Wechsler Memory Scale (Wechsler, 1987). Participants must also have an MMSE score between 24 and 30 and a CDR of 0 (memory box score must be 0). CN participants were considered CN based on an absence of significant impairment in cognitive functions or daily living activities.

#### 2.3.4. Mild cognitive impairment

Participants were classified as mild cognitive impairment (MCI) if they expressed subjective memory concern, with a score below the education-adjusted cutoffs on the Logical Memory II subscale from the Wechsler Memory Scale. The same MMSE score range as CN was used for the MCI group. Participants must have a global CDR of 0.5 and the memory box score must be at least 0.5. General cognition and functional performance of the MCI participants must

be sufficiently preserved such that clinical diagnosis of AD could not be made.

### 2.3.5. Alzheimer's disease

Participants categorized as AD were excluded from this study, to ensure the focus on early cognitive decline. In brief, participants were considered AD if they scored below the education-adjusted cutoff of the Wechsler Memory Scale, had an MMSE score between 20 and 24, and had global CDR  $\geq 0.5$  (Weiner et al., 2017).

### 2.4. Genotyping

A 7 mL sample of blood was taken in ethylenediaminetetraacetic acid-containing vacutainer tubes and genomic DNA was extracted at Cogenics (now Beckman Coulter Genomics) using the QIAamp DNA Blood Maxi Kit (Qiagen, Inc., Valencia, CA) following the manufacturer's protocol. All DNA extraction and genotyping was done blinded to group assignment. The 2 single nucleotide polymorphisms (rs429358, rs7412) that define the  $\epsilon 2$ ,  $\epsilon 3$ , and  $\epsilon 4$  alleles of the apolipoprotein E (*APOE*) were genotyped by polymerase chain reaction amplification and *HhaI* restriction enzyme digestion. The genotype was resolved on 4% MetaPhor gel and visualized by ethidium bromide staining.

### 2.5. Amyloid PET

Amyloid PET data were used to categorize participants to  $A\beta+$  and  $A\beta-$  groups. Amyloid PET analysis was performed according to UC Berkeley PET methodology for quantitative measurement (Baker et al., 2017a; Landau et al., 2014, 2015; Schöll et al., 2016). Participants were imaged by Florbetapir ( $^{18}\text{F}$ -AV-45; Avid). Six 5-minute frames of AV45 were acquired. All frames were co-registered to frame 1 using NeuroStat "mcoreg" module with rigid body translation and 6 degrees of freedom. All frames were averaged into a single image and reoriented into a  $160 \times 160 \times 96$  voxel image grid with 1.5 mm voxels. The reorientation was performed so that the anterior-posterior axis of the subject is parallel to the anterior-posterior commissure line.

### 2.6. Amyloid PET analysis

PET images were then co-registered on T1w MRI using the mutual information algorithm in SPM5 with default setting to align brain parcellation boundaries. The MRI and PET images were acquired within 3 months. Quantitative measurement was done based on standardized uptake value ratio (SUVR). The mean tracer uptakes in the main 4 cortical regions (frontal, anterior/posterior cingulate, lateral parietal, lateral temporal) were calculated. The mean of the whole cerebellum was also measured as the reference. Then, the whole cortical SUVR was calculated by averaging the mean of tracer uptake across the 4 cortical regions and dividing by the whole cerebellum reference region.

### 2.7. Tau PET and analysis

Tau PET was also collected by Flortaucipir ( $^{18}\text{F}$ -AV-1451). In this study, only the tau uptake in entorhinal region, which corresponds to the Braak stage 1 (Braak and Braak, 1996), was used to assess the correlation between PVS volume and early AD pathology. Similar pre-processing to amyloid PET was performed to measure tau PET SUVR in the entorhinal region. The tau PET values were normalized using cerebellar gray matter intensity.

For both amyloid and tau measurements, the analyzed PET from ADNI was used in this study (AV1451 version 05-12-2020 and AV45 version 08-09-2018). The technical details and reference metrics

are described in ADNI-3 documents and associated publications (Baker et al., 2017a,b; Braak and Braak, 1991; Brendel et al., 2015; Chen et al., 2015; Clark et al., 2011; Diedrichsen, 2006; Jagust et al., 2009; Joshi et al., 2012; Kepe, 2013; Landau et al., 2012, 2013a,b, 2014, 2015; Maass et al., 2017; Mormino et al., 2009; Reilhac et al., 2000; Schöll et al., 2016).

### 2.8. Cerebral spinal fluid biomarkers

CSF  $A\beta_{40}$ , CSF  $A\beta_{42}$ , and tau and phosphorylated Tau181 (p-Tau) measurement were completed using the Roche Elecsys Cobas e 601 fully automated immunoassay platform at the ADNI biomarker core (University of Pennsylvania). CSF biomarker samples were acquired in the 30-day interval of the imaging visit. All samples were aliquoted and stored at  $-80^\circ\text{C}$  until assay. A 2-dimensional ultra-performance liquid chromatography tandem mass spectroscopy platform was used (Kang et al., 2015; Korecka et al., 2014), which was calibrated with a surrogate calibrator matrix prepared from artificial CSF plus 4 mg/mL bovine serum albumin.

### 2.9. Magnetic resonance imaging

MRI imaging of the ADNI-3 was done exclusively on 3T scanners (Siemens, Philips, and GE) using a standardized protocol. Three-dimensional (3D) T1w with  $1\text{ mm}^3$  resolution was acquired using an MPRAGE sequence (on Siemens and Philips scanners) and FSPGR (on GE scanners). For FLAIR images, a 3D sequence with similar resolution as T1w images was acquired, which provided the opportunity for accurate intra-subject intermodal co-registration. MPRAGE T1w MRI scans were acquired using the following parameters: time of repetition (TR) = 2300 ms, time of echo (TE) = 2.98 ms, field of view (FOV) =  $240 \times 256\text{ mm}^2$ , matrix =  $240 \times 256$  (variable slice number), TI = 900 ms, flip angle = 9, effective voxel resolution =  $1 \times 1 \times 1\text{ mm}^3$ . The FSPGR sequence was acquired using sagittal slices, TR = 7.3 ms, TE = 3.01 ms, FOV =  $256 \times 256\text{ mm}^2$ , matrix =  $256 \times 256$  (variable slice number), TI = 400 ms, flip angle = 11, effective voxel resolution =  $1 \times 1 \times 1\text{ mm}^3$ . 3D FLAIR images were acquired using sagittal slices, TR = 4800 ms, TE = 441 ms, FOV =  $256 \times 256\text{ mm}^2$ , matrix =  $256 \times 256$  (variable slice number), TI = 1650 ms, flip angle = 120, effective voxel resolution =  $1 \times 1 \times 1.2\text{ mm}^3$ .

### 2.10. MRI preprocessing and brain parcellation

T1w preprocessing and parcellation was done using the FreeSurfer (v5.3.0) software package, which is freely available (Fischl, 2012), and data processing using the Laboratory of Neuro Imaging (LONI) pipeline system (<http://pipeline.loni.usc.edu>) (Dinov et al., 2009, 2010; Moon et al., 2015; Torri et al., 2012), similar to Sepehrband et al. (2018) and Sta Cruz et al., 2019. Brain volume and white matter mask were derived from the Desikan-Killiany atlas (Desikan et al., 2006). The parcellation was performed as part of the *recon-all* module of the FreeSurfer, which uses an atlas-based parcellation approach. Prior to parcellation, *recon-all* applies the following pre-processing steps: motion correction, non-uniform intensity normalization, Talairach transform computation, intensity normalization, and skull stripping (Fischl et al., 1999, 2002, 2004a,b; Dale et al., 1999; Desikan et al., 2006; Fischl and Dale, 2000; Reuter et al., 2010, 2012; Reuter and Fischl, 2011; Segonne et al., 2004, 2007; Sled et al., 1998; Waters et al., 2018).

FLAIR images of each participant were corrected for non-uniform field inhomogeneity using N4ITK module (Tustison et al., 2010) of Advanced Normalization Tools (ANTs) (Avants et al., 2009). FLAIR images were then co-registered to T1w images using *antsIntermodalityIntrasubject* ANTs module.

White matter regions from FreeSurfer *recon-all* outputs were used to study PVS across white matter region. FreeSurfer uses Desikan-Killiany atlas (Desikan et al., 2006) to parcellate cortical area into 68 regions and also provides parcellation of the corresponding underlying white matter regions, which were used in this study. The CSO-WM region of the FreeSurfer output was also used to ensure a complete coverage of the white matter. White matter regions were extracted from *aparc* parcellation of the FreeSurfer *recon-all* pipeline that is stored as *wmparc*. These white matter regions are listed in Supplementary File 3.

### 2.11. Mapping perivascular spaces

PVSs were mapped from T1w images and then white matter hyperintensities, which were falsely segmented as PVS, were excluded using FLAIR images. PVS segmentation was done using an automated and highly reliable quantification technique that we developed and validated (Sepehrband et al., 2019a). In brief, after preprocessing the data, T1w images were filtered using an adaptive non-local mean filtering technique (Manjón et al., 2010). The non-local mean technique measures the image intensity similarities by considering the neighboring voxels in a blockwise fashion, where the filtered image is  $\sum_{x_i \in V_i} \omega(x_i, x_j) u(x_j)$ . For each voxel ( $x_j$ ) the weight ( $\omega$ ) is measured using the Euclidean distance between 3D patches. The adaptive non-local mean filtering technique adds a regularization term to the above formulation to remove bias intensity of the Rician noise observed in MRI. Therefore the expected Euclidean distance between 2 noisy patches  $N_i$  and  $N_j$  is defined as:  $d(N_i, N_j) = u_0(N_i) - u_0(N_j)^2 + 2\sigma^2$ , where  $d(N_i, N_j) = 2\sigma^2$  if  $N_i = N_j$ . The Rician noise of the MRI images, calculated using robust noise estimation technique presented by Wiest-Daesslé et al., 2008, was used as the noise level for non-local filtering (Manjón et al., 2010). To preserve PVS voxels while removing the noise, filtering was applied only on high-frequency spatial noises. This was achieved by using a filtering patch with a radius of 1 voxel, which removes the noise at a single-voxel level and preserves signal intensities that are spatially repeated (Manjón et al., 2010).

Subsequently, we applied a Frangi filter (Frangi et al., 1998) to T1w using the Quantitative Imaging Toolkit (Cabeen et al., 2018). The Frangi filter estimates a vesselness measure for each voxel  $V(s)$  from eigenvectors  $\lambda$  of the Hessian matrix  $H$  of the image:

$$V(s) = \begin{cases} 0 & \text{if } \lambda_2 > 0 \text{ or } \lambda_3 > 0, \\ \left(1 - \exp\left(-\frac{R_A^2}{2\alpha^2}\right)\right) \exp\left(-\frac{R_B^2}{2\beta^2}\right) \left(1 - \exp\left(-\frac{S^2}{2c^2}\right)\right) & \text{otherwise} \end{cases}$$

where  $R_A = \frac{|\lambda_1|}{|\lambda_2|}$ ,  $R_B = \frac{|\lambda_1|}{\sqrt{|\lambda_2 \lambda_3|}}$ ,  $S = H$ .

Default parameters of  $\alpha = 0.5$ ,  $\beta = 0.5$ , and  $c$  were used, as recommended in Frangi et al (1998). The parameter  $c$  was set to half the value of the maximum Hessian norm. Frangi filter estimated vesselness measures at different scales and provided the maximum likelihood. The scale was set to a large range of 0.1–5 voxels in order to maximize the vessel inclusion. The output of this step is a quantitative map of vesselness in regions of interest (ROIs) and is taken to be the maximum across scales, as suggested in the original paper (Frangi et al., 1998). The range corresponds to specific levels in scale space that are searched for tubular structure feature detector. Thus, the outputs across voxels comprise vesselness measured across a range of filter scales. Then vesselness threshold of 0.00002 was used to segment the PVS voxels (note that original PVS segmentation reported the scaled thresholds—the raw threshold is reported here for the ease of replication). For each segmented voxel, corresponding

FLAIR voxels were checked, and if the FLAIR voxel value was a white matter hyperintensity, then the voxel was excluded from the final PVS mask. To check for white matter hyperintensities, PVS voxels that were in the top 10 percentile of the FLAIR signal distribution were excluded from the PVS mask. Supplementary Fig. 1 shows an example of the PVS map of one of the study participants.

PVS segmentation performance was assessed on a sub-set of data. Twenty-five participant data were randomly chosen and PVS masks were manually corrected to include undetected PVS and exclude incorrect PVS. Then, the performance of the automated segmentation technique with and without white matter hyperintensity correction was assessed using 3 metrics: (1) the sensitivity (also known as recall), (2) the precision (also known as positive predictive value), and (3) F1 score (also known as Dice similarity coefficient), defined as:

$$\text{Sensitivity} = \frac{TP}{TP + FN}, \text{ Precision} = \frac{TP}{TP + FP}, \text{ F1 score} = \frac{2TP}{2TP + FP + FN}$$

where TP (True Positive) denotes the number of segmented PVS voxels by algorithm which also belong to PVS voxels of the ground truth; FN (False Negative) denotes the number of segmented background voxels by algorithm which belong to PVS of the ground truth; FP (False Positive) denotes the number of segmented PVS voxels by algorithm which belong to background of ground truth.

The sensitivity of the segmentations to PVS voxels was  $98 \pm 2\%$  (mean  $\pm$  standard deviation [M  $\pm$  SD]) for the automated mapping with and without FLAIR correction. The precision of the automated technique with and without FLAIR correction was  $61 \pm 17\%$  (M  $\pm$  SD) and  $93 \pm 5\%$  (M  $\pm$  SD), respectively. F1 score of the automated technique with and without FLAIR correction was  $74 \pm 14\%$  (M  $\pm$  SD) and  $95 \pm 3\%$  (M  $\pm$  SD), respectively. Evaluation results highlight the importance of the post-processing correction with FLAIR. This is because of the large presence of non-PVS hypointense signal in aging population, which could drastically affect the precision of the automated technique on T1w alone data.

T1w images were registered to the ANTs template non-linear registration module (Avants et al., 2009, 2011), and the same transformation matrix was applied to PVS masks. PVS masks of all participants were transformed to the template space. Then the normative PVS was generated for each of the CN and MCI groups (Fig. 1). The normative PVS was generated by averaging the binary PVS masks (i.e., sum of all PVS masks divided by the group size). Two ROIs were then drawn on the template to enable statistical analysis of the PVS presence. The first ROI was drawn in the anterosuperior medial temporal lobe (asMTL), and the second on the CSO-WM. The ROIs were registered back into each subject's space. Then, the volume of PVS in those regions was divided by the total ROI volume to extract PVS volume fraction. CSO-WM was selected because this region has been historically used as the clinical ROI to assess PVS (Wardlaw et al., 2020a,b). The asMTL region was included following the qualitative observation of the PVS normative map in normal aging group and individuals with cognitive deficit (Fig. 1). The PVS observed in asMTL mainly corresponds to anterior temporal arteries and their sub-branches, penetrating from the anterior part of the temporal lobe along the anterior-posterior axis (Supplementary Fig. 2).

All FLAIR and T1w MRI images were manually checked for misalignment and post-processing failure, randomly and blind to clinical and neuroimaging measures. A total of 37 participants were excluded after the quality control.

We observed MRI manufacturer difference across PVS measures, in which PVSs were consistently underestimated in Philips compared to other scanners ( $p < 0.01$  across all comparisons).

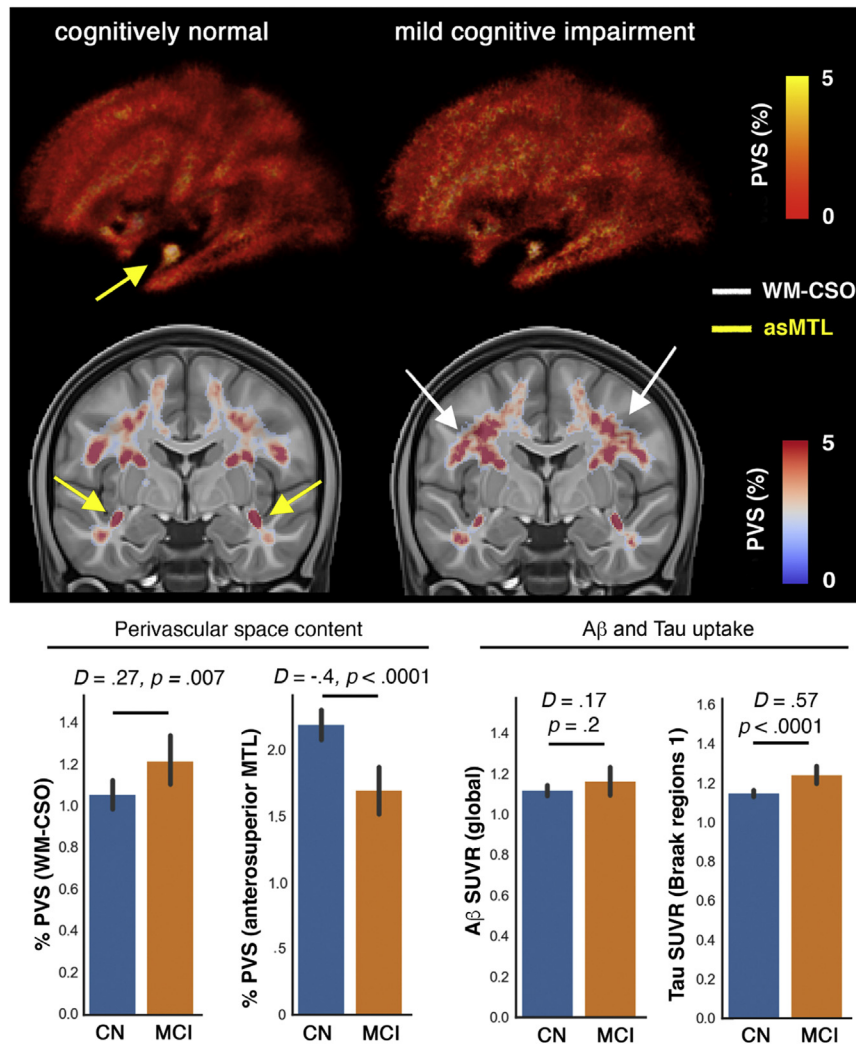


**Fig. 1.** Maps of the PVS in CN ( $n = 424$ ) and mild cognitively impaired ( $n = 173$ ) participants of ADNI-3. Normative maps of PVS across CN and MCI are presented, which were obtained by averaging PVS maps across the group (presenting percentage of overlapping PVS content across group). Overall, a higher amount of PVS was observed in global white matter and specifically in the CSO-WM region of the MCI participants. Surprisingly, in the MCI group, a lower amount of PVS was observed in asMTL white matter. As comparison references, total SUVR of cerebral A $\beta$ , and Tau PET SUVR in the regions associated with Braak stage 1 (i.e., entorhinal cortex) were included.  $D$  and  $p$  values are Cohen's  $d$  (effect size) and  $p$ -value of the group differences, measured using estimation statistics. Abbreviations: A $\beta$ , amyloid beta; ADNI-3, Alzheimer's Disease Neuroimaging Initiative 3; asMTL, anterosuperior medial temporal lobe; CN, cognitively normal; CSO-WM, centrum semi-ovale of the white matter; MCI, mild cognitive impairment; PET, positron emission tomography; PVS, perivascular space; SUVR, standardized uptake value ratio.

Therefore, 2 post hoc tests were performed: (1) manufacturer was included in the regression model as covariate. No statistically significant contribution from scanner manufacturer was observed in any statistical model (all  $p$ -value  $\geq 0.55$ ). (2) Statistical analysis was repeated, excluding 51 participants that were scanned with the Philips scanner. Statistical conclusions were equivalent to those from the full dataset when images from Philips scanner were excluded (Supplementary File 2).

## 2.12. Statistical analysis

Table 1 summarizes study participants' demographic and clinical information. To assess the PVS volume fraction differences, we used estimation statistics when comparing CN and MCI group differences (Ho et al., 2019). To this end, we estimated the group mean difference by calculating the unpaired Cohen's  $d$  effect size and the confidence interval between the PVS volume fraction of CN and MCI groups. To calculate the confidence interval of the effect size, 5000 bootstrap samples were taken. The confidence interval was bias-

corrected and accelerated (Ho et al., 2019). We also reported 2-sided  $p$ -value of Mann-Whitney test, which was reported as the likelihood of observing the effect size, if the null hypothesis of zero difference is true. Secondary statistical analyses were performed to incorporate potential confounds. To this end, one-way analysis of covariates (ANCOVA) was conducted to determine a statistically significant difference between CN and MCI individuals on the PVS volume fraction, controlling for age, sex, and years of education using a linear model. An interaction between cognitive status and sex was also included in the model to examine if PVS group differences in cognitive status are different between male and female individuals. PVS estimates were calculated as a volume fraction, defined as the volume of PVS in the region. For domain-specific analysis, a similar approach with the same formulation was used, but with the difference that CDR was used to make 2 groups: participants with no cognitive deficit (i.e., CDR = 0) and participants with mild cognitive deficit (i.e., CDR = 0.5). PVS was also assessed across 68 white matter regions of the Desikan-Killiany atlas (Desikan et al., 2006), which were obtained using *recon-all* module

**Table 1**  
Participant summary information

Measures	Cognitively normal	MCI	Statistical <i>p</i> -value
<i>N</i>	423	173	
Female, <i>n</i> (%)	252 (59%)	73 (42%)	0.0001
Age (y)	73.04 ± 7.36	75.56 ± 8.16	0.0003
Education (y)	16.90 ± 2.25	15.98 ± 2.78	0.00007
Brain volume (mm <sup>3</sup> )	1,064,574 ± 107,460	1,051,535 ± 106,529	0.358
CDR global <sup>a</sup>	0.0 (0.0)	0.5 (0.0)	3 × 10 <sup>-168</sup>
CDR memory <sup>a</sup>	0.0 (0.0)	0.5 (0.0)	6 × 10 <sup>-133</sup>
CDR sum-of-boxes <sup>a</sup>	0.0 (0.0)	1.0 (1.5)	3 × 10 <sup>-86</sup>
MMSE <sup>a</sup>	29.0 (1.0)	29.0 (3.0)	9 × 10 <sup>-15</sup>
<i>APOE</i> status, <i>n</i> (%) <sup>e</sup>			
ε3/ε3	212 (66%)	78 (61%)	
ε3/ε4	99 (31%)	37 (29%)	
ε4/ε4	10 (3%)	12 (9%)	
Mean Aβ PET (global SUVR) <sup>b</sup>	1.11 ± 0.17	1.16 ± 0.27	0.043
Mean Tau PET (entorhinal region) <sup>c</sup>	1.10 ± 0.13	1.20 ± 0.23	0.000014
History of hypertension, <i>n</i> (%) <sup>d</sup>	91 (34%)	44 (52%)	0.002
Systolic pressure (mm Hg)	133.9 ± 17.8	134.1 ± 18.0	0.863
Diastolic pressure (mm Hg)	75.0 ± 9.6	73.4 ± 8.4	0.051

Values are expressed as mean ± SD or frequency (percent).

Key: Aβ, amyloid beta; *APOE*, apolipoprotein E; CDR, clinical dementia rating; CN, cognitively normal; IQR, interquartile range; MCI, mild cognitive impairment; MMSE, Mini-Mental State Examination; PET, positron emission tomography; SUVR, standardized uptake value ratio.

<sup>a</sup> Values are expressed as median (IQR) (normality hypothesis was rejected with D'Agostino and Pearson's test; Pearson et al., 1977).

<sup>b</sup> *n* = 259 participants had Florbetapir AV45 Aβ PET data: *n*(CN) = 171, *n*(MCI) = 59.

<sup>c</sup> *n* = 345 participants had Flortaucipir AV1451 Tau PET data: *n*(CN) = 240, *n*(MCI) = 79.

<sup>d</sup> *n* = 378 participants (269 CN, 86 MCI) had data about history of hypertension.

<sup>e</sup> *n* = 508 participants had *APOE* status data, *n* = 60 with *APOE* ε2 were excluded in genotype analysis.

of the FreeSurfer. The Benjamini-Hochberg procedure with a false discovery rate of 0.05 was used to correct for multiple comparisons. All ANCOVA statistical results are included in [Supplementary File 3](#) and the significant regions are reported in the text. Throughout the manuscript raw *p*-values are reported.

The association between PVS volume fraction and tau pathology, as measured by PET, was investigated. For tau PET analysis, regional SUVRs in medial temporal lobe regions associated with early AD pathology were investigated. In particular, we examined whether PVS volume fraction of asMTL is correlated with tau uptake in regions with early AD pathology: entorhinal cortex (ERC) and parahippocampal cortex (PHC). The correlation between PVS volume fraction and tau uptake was also compared in ERC and PHC. For these analyses, we formulated a linear regression model to investigate whether PVS volume fraction is a predictor of Flortaucipir (AV-1451) SUVR, adjusting for age, sex, education, and brain size. An ordinary least square fitting was used to fit the linear regression to the data using StatsModels Python library. A secondary analysis was also performed including the continuous unthresholded Aβ SUVR as a covariate to compare the effect size of PVS volume fraction against Aβ SUVR.

We then looked into possible explanations for PVS volume fraction mean differences between CN and MCI groups, including amyloid PET, *APOE* status, and cardiovascular measures. For the amyloid PET analysis, participants were categorized into CN and MCI with and without amyloid presence, which was defined by a cutoff at SUVR of 1.1 (Baker et al., 2017a; Landau et al., 2014, 2015; Schöll et al., 2016). Mean PVS volume fractions were then compared across Aβ- and Aβ+ groups, correcting for age, sex, and education. When the overall association between vascular and PVS volume fraction and amyloid load was assessed, the continuous unthresholded Aβ SUVR values were used. Similar estimation statistics framework was used for *APOE* status comparison and cardiovascular measures. For the *APOE*-ε4 carrier status analysis, participants were categorized into 3 groups based on the number of *APOE* ε4 allele repeats: 0 for ε3/ε3, 1 for ε3/ε4, and 2 for ε4/ε4. Participants with *APOE*-ε2 allele were excluded from genotype analysis as it was shown to be a protective carrier (Panza et al., 2000; Qiu et al., 2004). A secondary analysis was done including

*APOE*-ε2 allele, which resulted to the same conclusion (no association was found).

Because of the pathological changes in blood vessels observed in hypertension as well as the cerebrovascular response to the blood levels of oxygen and carbon dioxide, which are 2 primary determinants of ventilation (Battisti-Charbonney et al., 2011), we explored the contributions of blood pressure and respiratory rate to the PVS. Available cardiovascular risk factors including history of hypertension and vital signs (systolic and diastolic pressures, respiration rate, and temperature) were used as independent variables to explain the variation of PVS volume fraction. Similar linear regression modeling as above was used for this purpose, correcting for age, sex, and education. The Benjamini-Hochberg procedure with a false discovery rate of 0.05 was used to correct for multiple comparisons (Fig. 6 and [Supplementary File 4](#)).

Hippocampal volumes were extracted from FreeSurfer outputs and compared across groups. Given the significant hippocampal volume difference (CN > MCI:  $p = 5 \times 10^{-12}$ ), additional statistical analysis was performed, including hippocampal volume as covariate for MTL results. PVS difference of the asMTL remained significantly different between CN and MCI after incorporating hippocampal volume as a covariate: left asMTL (CN > MCI:  $F(1, 532) = 6.11, p = 0.013$ ) and right asMTL (CN > MCI:  $F(1, 532) = 4.51, p = 0.03$ ).

Finally, given the significant difference in the age and sex distribution between the CN and MCI groups (Table 1), a secondary analysis was done on an age- and sex-matched subgroup. This subgroup included a random sample of participants with the same sex and comparable age equally distributed in the CN and MCI groups. The demographic and clinical information about the age- and sex-matched subgroup is summarized in Table 2.

### 3. Results

A higher total amount of PVS was observed in the normative PVS map of MCI participants compared to CN participants (Fig. 1). The increased PVS in MCI compared to CN participants was most evident in the CSO-WM. Surprisingly, PVS percentage on the normative template was notably lower in MCI compared to CN in the asMTL (yellow arrow in Fig. 1). The tau SUVR in the ERC was

**Table 2**  
Participant summary information of the age- and sex-matched subgroup

Measures	Cognitively normal	MCI	Statistical <i>p</i> -value
N	173	173	
Female, n (%)	73 (42%)	73 (42%)	1
Age (y)	75.57 ± 8.06	75.56 ± 8.16	0.984
Education (y)	16.85 ± 2.51	15.98 ± 2.78	0.004
Brain volume (mm <sup>3</sup> )	1,085,078 ± 107,438	1,051,535 ± 106,529	0.469
CDR global <sup>a</sup>	0.0 (0.0)	0.5 (0.0)	3 × 10 <sup>-86</sup>
CDR memory <sup>a</sup>	0.0 (0.0)	0.5 (0.0)	5 × 10 <sup>-65</sup>
CDR sum-of-boxes <sup>a</sup>	0.0 (0.0)	1.0 (1.5)	1 × 10 <sup>-41</sup>
MMSE <sup>a</sup>	29.0 (1.25)	29.0 (3.0)	3 × 10 <sup>-7</sup>

Values are expressed as mean ± SD or frequency (percent).

Key: CDR, clinical dementia rating; IQR, interquartile range; MCI, mild cognitive impairment; MMSE, Mini-Mental State Examination; SD, standard deviation.

<sup>a</sup> Values are expressed as median (IQR) (normality hypothesis was rejected with D'Agostino and Pearson's test; Pearson et al., 1977).

significantly higher in MCI compared to CN participants (Cohen's  $d = 0.6$ ,  $p = 0.0014$ ), while group differences in global A $\beta$  SUVR were not observed (Cohen's  $d = 0.17$ ,  $p = 0.2$ ). To enable statistical analysis to assess the association of asMTL with demographic, cognitive, and neuropathological measurement, an ROI of the asMTL was drawn on the study T1w MRI template and was used to estimate PVS volume fraction in asMTL. Other regions of the MTL white matter are included in the Desikan-Killiany atlas (Desikan et al., 2006) used in this study.

No asymmetry was observed in CSO-WM ( $p = 0.6$ ) and therefore the total CSO-WM was used for the rest of the analysis. PVS volume fraction of the CSO-WM was higher in MCI compared to CN (Fig. 2D:  $p = 0.007$  and Cohen's  $d = 0.27$ ). We found a significant effect of age

on PVS volume fraction of CSO-WM ( $F(1, 532) = 33.6$ ,  $p = 1 \times 10^{-8}$ ), whereas we did not find any significant effect of the cognitive status ( $p = 0.08$ ) or sex ( $p = 0.11$ ) individually. However, we observed a significant effect of the interaction of cognitive status and sex on PVS volume fraction of the CSO-WM after controlling for age and years of education ( $F(1, 532) = 4.05$ ,  $p = 0.044$ ). When PVS volume fraction of CSO-WM was assessed separately in male and female groups, we found a significant effect of cognitive status on PVS volume fraction after controlling for age and years of education in females (MCI > CN:  $F(1, 280) = 10.63$ ,  $p = 0.001$ ), but no significant difference between CN and MCI in males ( $F(1, 249) = 0.02$ ,  $p = 0.88$ ). In the female group, the adjusted  $F$  ratio of the cognitive status was almost as high as the age effect on the PVS volume fraction ( $F(1,$

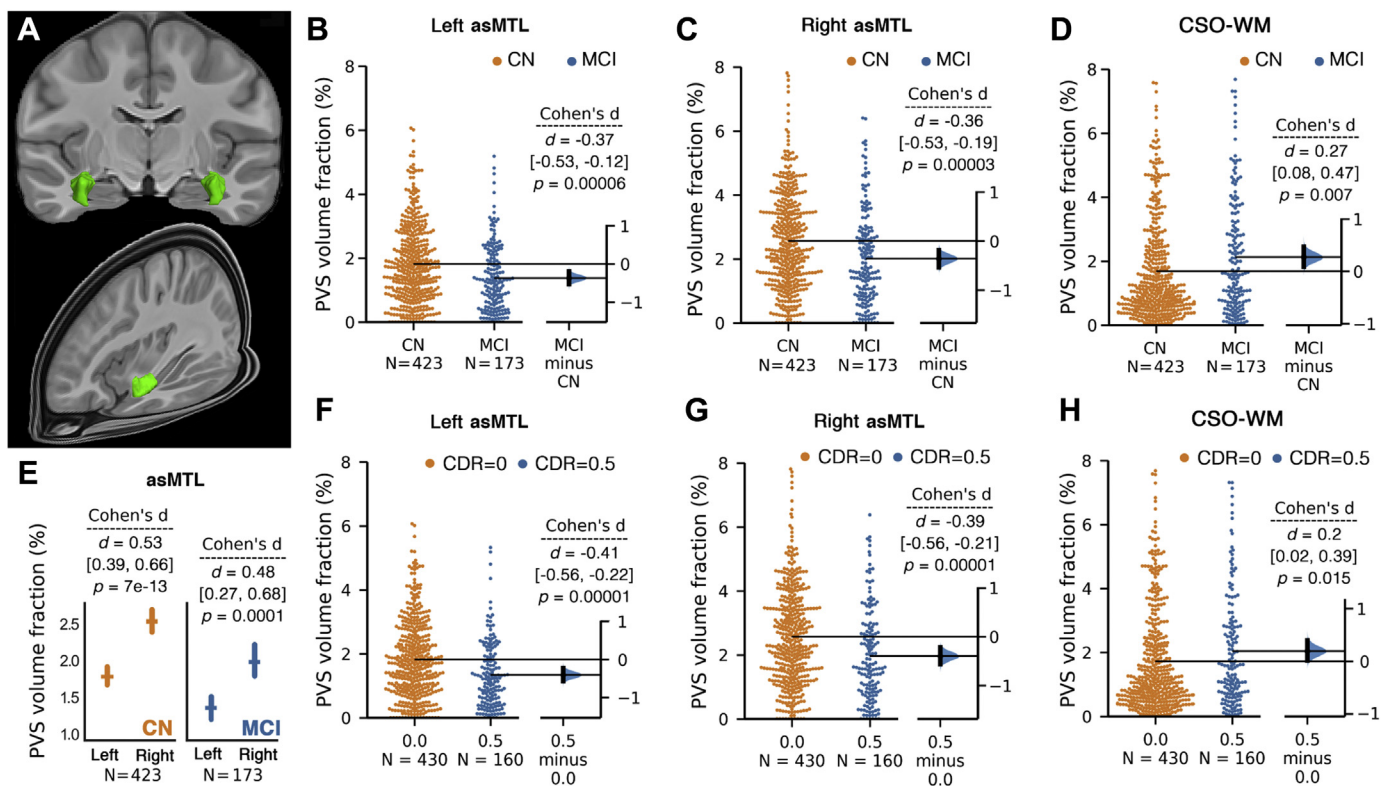


**Fig. 2.** PVS volume fraction in asMTL was significantly lower in MCI participants compared to CN. A 3D render of the asMTL on template space is presented in (A). Bilateral and significant PVS volume fraction differences between CN and MCI participants were observed in asMTL (B, C). Unpaired Cohen's  $d$  effect size and confident intervals were reported ( $d$  [CI]) for the group differences between CN and MCI using estimation statistics (Ho et al., 2019). Two-sided  $p$ -value of Mann-Whitney test was also reported. The PVS volume fraction in asMTL was asymmetrical across both CN and MCI groups (E); mean and standard errors are shown. Diagnostic group comparison on PVS volume fraction across the CSO-WM is shown in (D). (F–H) plots compare PVS volume fraction of the asMTL (F, H) and CSO-WM (H) when study participants were categorized based on CDR. Abbreviations: 3D, three-dimensional; asMTL, anterosuperior medial temporal lobe; CDR, clinical dementia rating; CN, cognitively normal; CSO-WM, centrum semi-ovale of the white matter; MCI, mild cognitive impairment; PVS, perivascular space.

280) = 14.66,  $p = 0.0001$ ). When PVS volume fraction of CSO-WM was assessed separately in CN and MCI participants, we observed a significantly higher PVS volume fraction in males compared to females ( $p = 0.0002$ , Cohen's  $d = 0.38$ ), but no sex difference in the MCI group ( $p = 0.99$ ).

The PVS volume fraction in the asMTL region was significantly higher in the right hemisphere compared to the left in both CN ( $p = 7 \times 10^{-13}$ ) and MCI ( $p = 0.0001$ ) groups (Fig. 2E). Therefore, statistical analyses were conducted separately for each hemisphere. A significantly lower PVS volume fraction in MCI compared to CN groups was observed (Fig. 2B and C) in both left ( $p = 0.00006$ ) and right ( $p = 0.00003$ ) asMTL. After correcting for age, sex, and years of education, the effect of cognitive status on PVS volume fraction remained significant in the left asMTL ( $F(1, 532) = 11.25$ ,  $p = 0.0008$ ), which explained a higher variance in the model compared to the effect of age on PVS volume fraction ( $F(1, 532) = 8.04$ ,  $p = 0.005$ ). No other covariate significantly affected the PVS volume fraction. Similarly in right asMTL, we found a significant effect of cognitive status on PVS volume fraction after correcting for age, sex, and years of education ( $F(1, 532) = 12.94$ ,  $p = 0.0003$ ), which explained a higher variance in the model compared to the effect of age on PVS volume fraction ( $F(1, 532) = 11.96$ ,  $p = 0.0006$ ). No other covariate significantly affected the PVS volume fraction.

When participants were categorized based on CDR scores (Fig. 2F and G), the same pattern was observed: PVS volume fraction of asMTL was significantly lower in participants with signs of cognitive deficit (CDR = 0.5) compared with CN individuals bilaterally (CDR = 0) (left asMTL:  $p = 0.00001$ , right asMTL:  $p = 0.00001$ ).

When regional analyses across white matter were performed on the effect of cognitive status on PVS volume fraction, 4 regions survived the multiple comparison correction and remained significantly different after correcting for age, sex, and years of education: left medial orbitofrontal region (MCI > CN),  $F(1, 532) = 3.93$ ,  $p = 0.048$ ; left pars opercularis (MCI > CN),  $F(1, 532) = 4.77$ ,  $p = 0.029$ ; left rostral middle frontal region (MCI > CN),  $F(1, 532) = 4.16$ ,  $p = 0.041$ ; and right entorhinal region (MCI < CN),  $F(1, 532) = 6.36$ ,  $p = 0.012$ . A complete list of statistical results is presented in [Supplementary File 3](#). In all these regions, the MCI group had higher PVS volume fraction than CN, except for the entorhinal region, where the CN group had higher PVS volume fraction, corroborating findings from the analysis of the asMTL region. No significant difference was observed in other regions of MTL. The asMTL difference was associated with hippocampal volume (left asMTL:  $F(1, 532) = 6.11$ ,  $p = 0.013$ ; right asMTL:  $F(1, 532) = 21.14$ ,  $p = 0.000005$ ; incorporating age, sex, and years of education as covariates), but not confounded by it. When hippocampal volume was included in the analysis, the PVS volume fraction difference between CN and MCI in asMTL remained statistically significant (left asMTL, CN > MCI:  $F(1, 532) = 6.11$ ,  $p = 0.013$ ; right asMTL, CN > MCI:  $F(1, 532) = 4.51$ ,  $p = 0.03$ ; incorporating age, sex, and years of education as covariates).

When the age- and sex-matched subgroup was analyzed (Table 2), similar conclusions were reached (i.e., CN participants presented higher PVS volume fraction in asMTL and lower PVS volume fraction in CSO-WM). In brief, PVS volume fraction of asMTL was significantly higher in CN compared to MCI: left asMTL, CN > MCI:  $F(1, 309) = 17.3$ ,  $p = 0.00004$ ; right asMTL, CN > MCI:  $F(1, 309) = 18.52$ ,  $p = 0.00002$ ; incorporating age, sex, and years of education as covariates. PVS volume fraction of CSO-WM was significantly higher in MCI compared to CN in females ( $F(1, 124) = 6.09$ ,  $p = 0.015$ ; incorporating age, sex, and years of education as covariates), but not males ( $F(1, 183) = 0.79$ ,  $p = 0.37$ ). In the regional analysis, same conclusions were made in the subgroup analysis for right entorhinal (MCI < CN:  $F(1, 341) = 10.04$ ,  $p = 0.002$ ) and left pars opercularis regions (MCI > CN:  $F(1, 341) = 5.17$ ,  $p = 0.023$ ), but

not left medial orbitofrontal and left rostral middle frontal regions, incorporating age, sex, and years of education as covariates.

PVS volume fraction in the asMTL was significantly associated with tau PET SUVR in the ERC, which is a pathological hallmark of AD in the first stages (Braak stages I: Braak and Braak, 1996). The association appeared to be lateralized, in which only the tau SUVR on the right ERC showed significant correlation with the PVS volume fraction of the ipsilateral white matter of the asMTL (Fig. 3B) (beta (SE) =  $-0.98$  (0.4),  $p = 0.014$ , corrected for age, sex, and education). Unlike ERC, we did not observe significant associations between asMTL PVS volume fraction and tau uptake in the HC or PHC bilaterally (Fig. 3C;  $p > 0.27$ ). We observed that PVS volume fraction was associated with tau uptake in regions associated with Braak I (i.e., ERC; Fig. 3F), but the association was weaker (and non-significant) for tau uptake in the parahippocampal region (Fig. 3F;  $p = 0.25$ ).

No significant associations between PVS volume fraction and tau or A $\beta$  SUVR were found in white matter regions associated with late Braak stages. We only observed a weak non-significant association between PVS volume fraction of medial orbitofrontal white matter and A $\beta$  SUVR of medial orbitofrontal cortex ( $F(1, 224) = 3.29$ ,  $p = 0.07$ ).

PVS volume fractions across different regions were independent of amyloid load or APOE  $\epsilon 4$  status (Figs. 4, 5). A second linear regression was performed using cerebral amyloid load values (A $\beta$  SUVR) as a predictor of PVS volume fraction, using age, sex, and years of education as covariates, which showed no significant relationship between A $\beta$  uptake and PVS volume fraction ( $p = 0.61$ ). The same conclusion was drawn when the analysis was performed on CN and MCI groups separately. No differences in mean PVS volume fraction between A $\beta$ - and A $\beta$ + participants were observed in MCI and CN participants (CN [left asMTL]:  $p = 0.75$ ; CN [right asMTL]:  $p = 0.98$ ; MCI [left asMTL]:  $p = 0.55$ ; MCI [right asMTL]:  $p = 0.16$ ; CN [CSO-WM]:  $p = 0.95$ ; MCI [CSO-WM]:  $p = 0.15$ ; [Supplementary Fig. 3](#)). We also observed no PVS volume fraction difference across participants with different APOE  $\epsilon 4$  repeats (Fig. 5).

When total asMTL PVS volume fraction and composite cerebral amyloid load values (A $\beta$  SUVR) were included in the same logistic regression model to predict the cognitive status (MCI vs CN), the asMTL PVS (beta (SE) =  $-0.33$  (0.1);  $t = -2.3$ ;  $p = 0.019$ ; lower in MCI) was a stronger predictor than that of PET SUVR (beta (SE) =  $2.26$  (1.2);  $t = 1.8$ ;  $p = 0.07$ ; higher in MCI), supporting the hypothesis that alterations in the supply and clearance of the asMTL is an early feature of AD-related cognitive decline. No association between PVS volume fraction and CSF biomarkers were found ([Supplementary File 5](#)). Continuous data of CSF A $\beta$ 1-42, A $\beta$ 1-40, tau and phosphorylated tau (p-Tau) were used for the association analysis, adjusting for age, sex, years of education, and brain size.

Finally, hypertension and vital sign relation with PVS measures were assessed (Fig. 6). Participants with a history of hypertension had significantly higher PVS volume fraction in the CSO-WM ( $p = 0.0007$ ) and significantly lower PVS volume fraction in the left asMTL ( $p = 0.006$ ). These differences were no longer statistically significant when age, sex, and years of education were included (the difference was mainly explained by age and years of education). We only noted a marginal difference between PVS volume fraction of the CSO-WM in female participants with and without history of hypertension (higher PVS volume fraction in female with history of hypertension:  $F(1, 163) = 3.59$ ,  $p = 0.05$ ). After exploring the vital signs (systolic, diastolic and pulse pressure, respiration rate, and temperature), we observed a significant inverse association between respiration rate and PVS volume fraction in the asMTL ( $p = 0.004$ , adjusted for age, sex, and education), in which tachypneic participants (respiration rate >20 per minute) had lower PVS



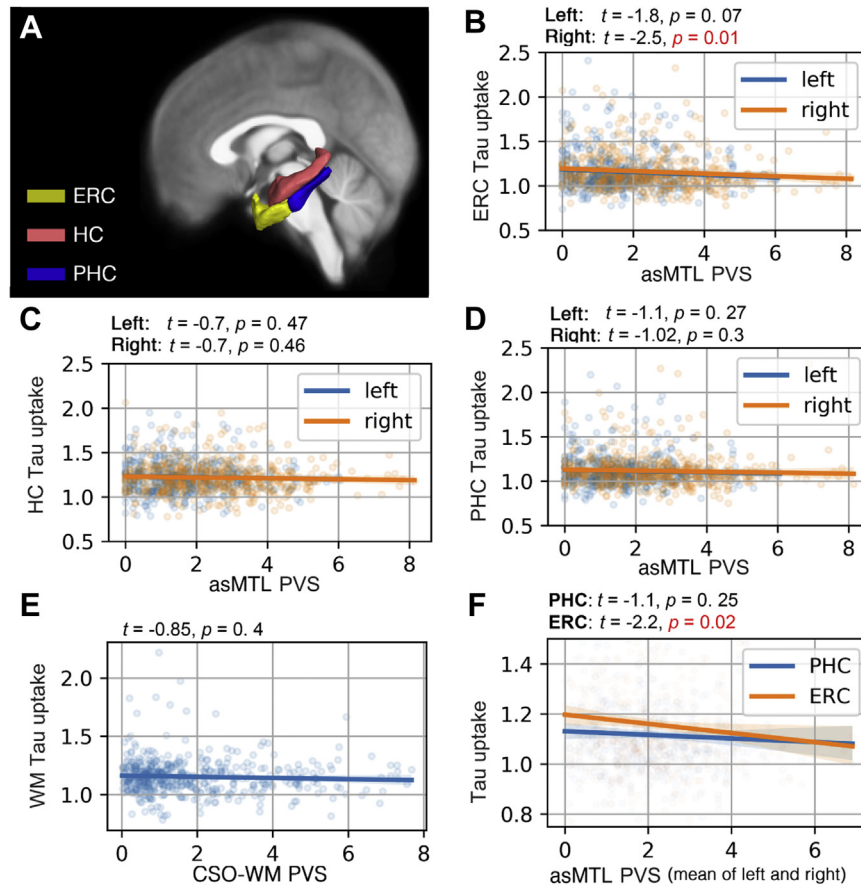


**Fig. 3.** PVS volume fraction was associated with early AD pathology. Studied regions of interest are shown in (A). PVS volume fraction of the asMTL was a predictor of Tau uptake (AV1451 PET Tau SUVR) in ERC (B) (right asMTL:  $p = 0.01$ , left asMTL:  $p = 0.07$ , corrected for age, sex, education, and brain size), in contrast with PVS volume fraction of the CSO-WM ( $p = 0.4$ ) (E). A non-significant correlation between PVS volume fraction of asMTL and Tau uptake in ERC and PHC was observed (C, D). Participants with lower PVS volume fraction in asMTL appeared to have higher amount of Tau in ERC. The correlation between asMTL PVS volume fraction and Tau SUVR was highest in regions involved in early AD pathology (i.e., ERC as per Braak stage I), and the association was weaker for PHC (F). The association analysis was performed in a subset of the population including participants with both Tau PET and MRI data ( $n = 319$ ;  $n(\text{CN}) = 240$ ,  $n(\text{MCI}) = 79$ ). Abbreviations: AD, Alzheimer's disease; asMTL, anterosuperior medial temporal lobe; CN, cognitively normal; CSO-WM, centrum semi-ovale of the white matter; ERC, entorhinal cortex; MCI, mild cognitive impairment; MRI, magnetic resonance imaging; PET, positron emission tomography; PHC, parahippocampal cortex; PVS, perivascular space; SUVR, standardized uptake value ratio; WM, white matter.

volume fraction in the asMTL. After including variables with statistically significant associations with PVS (i.e., history of hypertension and respiration rate) into the analysis of PVS difference by cognitive status (CN vs MCI), all statistical conclusions regarding cognitive group differences remained unchanged.

#### 4. Discussion

In this study, we examined the distribution of regional white matter PVS alterations in individuals with MCI and CN older adults. Our findings show that older adults with MCI present with alterations to the PVS, specifically in the asMTL and CSO-WM. PVS volume fraction was higher in the CSO-WM of individuals with MCI, and this effect was driven by females. Surprisingly, individuals with MCI showed lower PVS volume fraction in the asMTL, which was highly correlated with tau uptake in regions affected in the early stages of AD progression. Finally, individuals with a history of hypertension present with higher PVS volume fraction in the CSO-WM and lower PVS volume fraction in the asMTL.

PVS enlargement in the CSO-WM is a commonly used biomarker for cerebrovascular pathology (Doubal et al., 2010; Ishikawa et al., 2018). Overall, our results demonstrate significantly larger PVS volume fractions in the CSO-WM of individuals with MCI compared to elderly CN controls. Our results are consistent with previous

findings of PVS enlargement in the CSO-WM of patients with MCI (Chen et al., 2011), AD (Banerjee et al., 2017; Chen et al., 2011), and cerebral amyloid angiopathy (Charidimou et al., 2015, 2017), as well as normal aging (Charidimou et al., 2013; Doubal et al., 2010). Similar to previous evidence showing the PVS burden in the CSO-WM is greater in CN males compared to females (Ramirez et al., 2015), we observed that CN males present higher PVS volume fraction compared to CN females, whereas no significant difference was found between females and males in the MCI group. In fact, MCI females showed higher PVS volume fraction in the CSO-WM compared to CN females, reaching values comparable to both CN and MCI males. It is possible that the PVS volume fraction of male healthy controls appear similar to those found in male MCI patients due to a higher baseline level of PVS in healthy males compared to females. Nevertheless, whether the differences in PVS between males and females are related to hormonal effects on the perivascular flow, structural anatomical variations, and/or sex differences in astrocytic response to inflammation, remain to be explored (Ramirez et al., 2016).

The asMTL region presented an asymmetric distribution of PVS across the 2 hemispheres, with the right asMTL having a higher PVS volume fraction than the contralateral side, irrespective of cognitive status. This asymmetric pattern observed both in CN and in MCI groups suggests that a lateralization of PVS in asMTL is possibly a

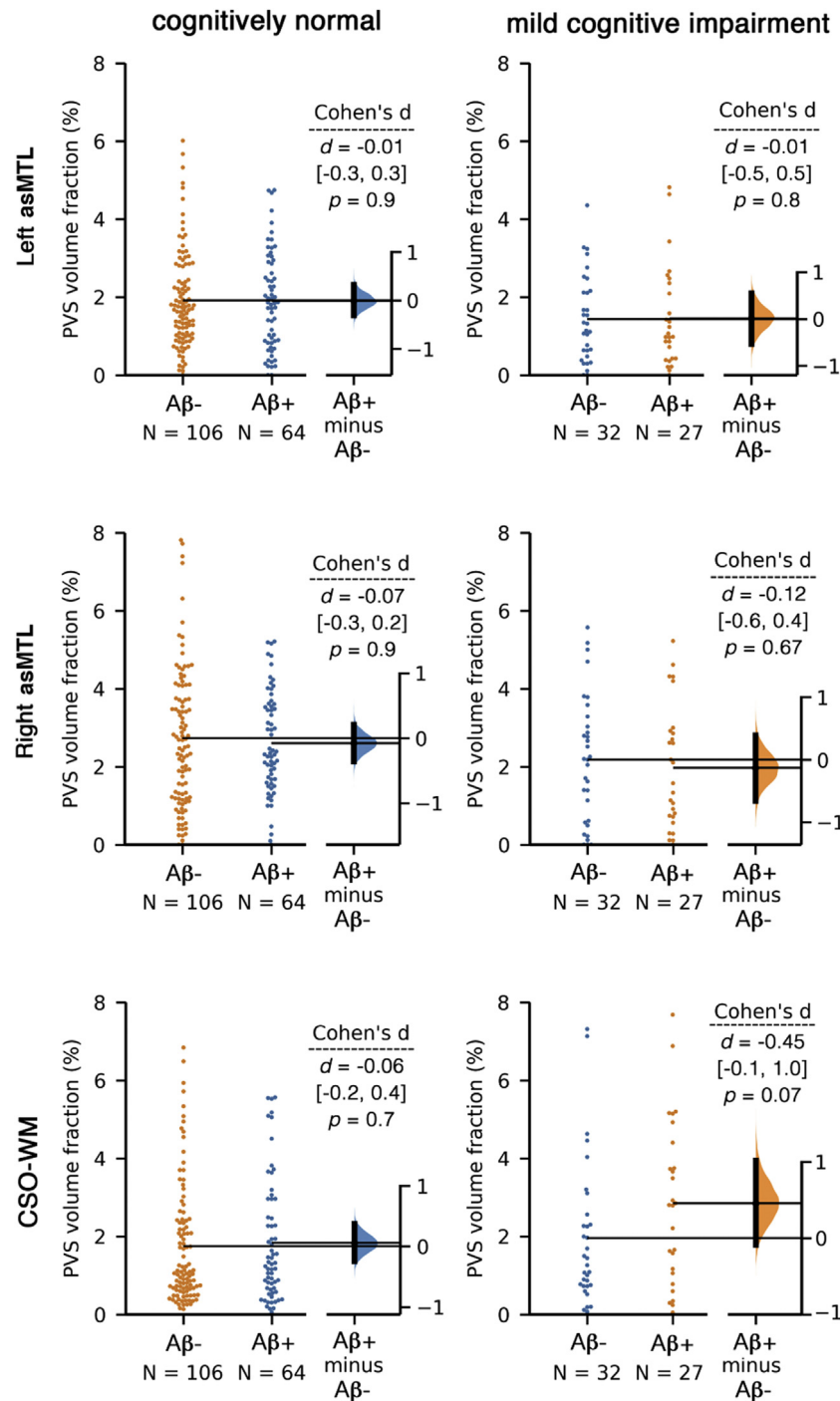


**Fig. 4.** PVS volume fraction of the asMTL and CSO-WM was not associated with the amyloid beta uptake, as measured by positron emission tomography. A $\beta$ -/+ categorization was applied based on Florbetapir cortical summary measurement (SUVR). Florbetapir cutoff of 1.11 using the whole cerebellum region was used as a reference. Equivalent statistical conclusions were drawn when we used a cutoff of 0.79 in a composite reference region including cerebellum, brainstem/pons, and eroded subcortical white matter. Linear regression analysis using A $\beta$  SUVR also showed no association between A $\beta$  uptake and PVS volume fraction ( $p = 0.61$ ). When regional values of A $\beta$  SUVR were used (instead of global SUVR), no associations were observed ( $p > 0.6$  for all tests). Abbreviations: A $\beta$ , amyloid beta; asMTL, anterosuperior medial temporal lobe; CSO-WM, centrum semi-ovale of the white matter; PVS, perivascular space; SUVR, standardized uptake value ratio.

normal physiological asymmetry and not related to pathology. [Perlmutter et al. \(1987\)](#) reported significantly higher cerebral blood flow and metabolic rate in the right superior temporal region of normal subjects using PET imaging, which was interpreted as a normal physiological asymmetry.

Within the medial temporal lobe, a region intimately connected with the limbic system and anatomically in contact with the

hippocampus, PVS content was associated with cognitive status in the white matter of the anterior superior MTL and right entorhinal region. The asMTL reflects the region adjacent to the anterior part of the superior temporal gyrus that receives blood supply from the anterior temporal arteries and their sub-branches ([Supplementary Fig. 2](#)) ([De Long, 1973](#)). Interestingly, we found the PVS volume fraction of the asMTL and right entorhinal region was significantly

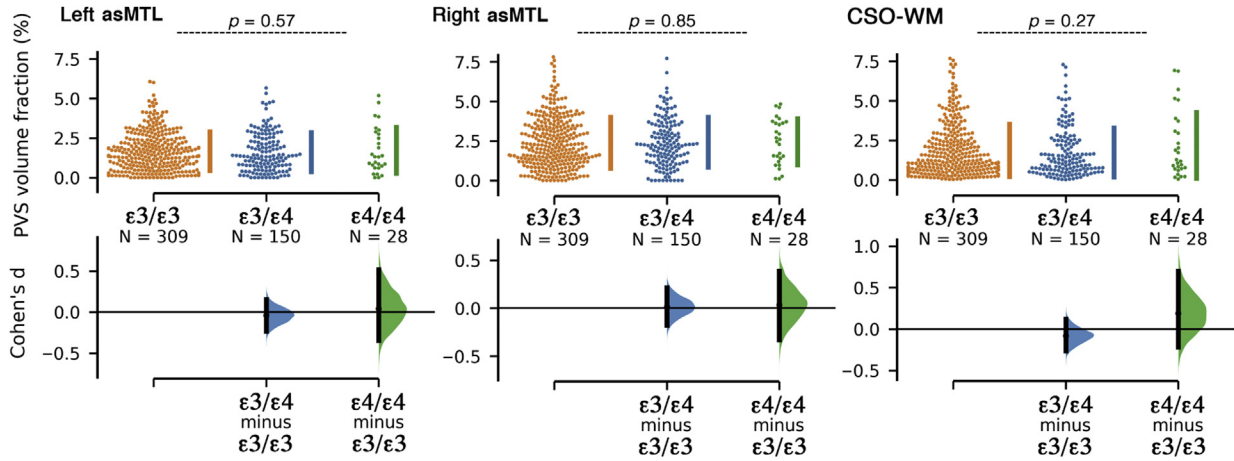


**Fig. 5.** PVS volume fraction of the asMTL and CSO-WM was not associated with *APOE*  $\epsilon 4$  allele repeats. Participants were categorized based on the number of *APOE*  $\epsilon 4$  allele repeats. Abbreviations: *APOE*, apolipoprotein E; asMTL, anterosuperior medial temporal lobe; CSO-WM, centrum semi-ovale of the white matter; PVS, perivascular space.

lower in patients with MCI compared to CN aging controls. This finding is in opposition to the conventional view that PVS dilation in cerebral white matter is a pathological feature of progressive glymphatic dysfunction in AD (Troili et al., 2020). However, previous studies of PVS enlargement in neurodegeneration have focused on the CSO-WM (Banerjee et al., 2017; Chen et al., 2011; Ramirez et al., 2015), basal ganglia (Banerjee et al., 2017; Chen et al., 2011; Ramirez et al., 2015; Zhu et al., 2010a), hippocampus (Chen et al., 2011), or global white matter (Zhu et al., 2010a) and there is limited evidence of regional differences in PVS content within the medial temporal lobe of individuals with MCI and AD.

In order to characterize the nature of the observed PVS alterations within the asMTL of MCI subjects, we explored associations

with more specific characteristics of AD pathology, such as deposition of amyloid beta plaques and tau neurofibrillary tangles, and genetic risk factors for AD. In this study, lower PVS volume fraction in the asMTL of patients with MCI was associated with higher tau PET SUVR but was independent of cerebral  $A\beta$  PET SUVR and *APOE4* status. This association with tau was found in the ERC, a region implicated in the pre-clinical stages of AD (Braak stages I) (Braak and Braak, 1991). The lower amount of PVS in the asMTL of individuals with MCI was concomitant with pathological alterations unique to the neurodegenerative processes that characterize early stages of AD progression. A previous cross-sectional study of  $A\beta$  deposition using PET in patients with MCI and AD similarly found no association between PVS content and  $A\beta$  uptake (Banerjee et al.,

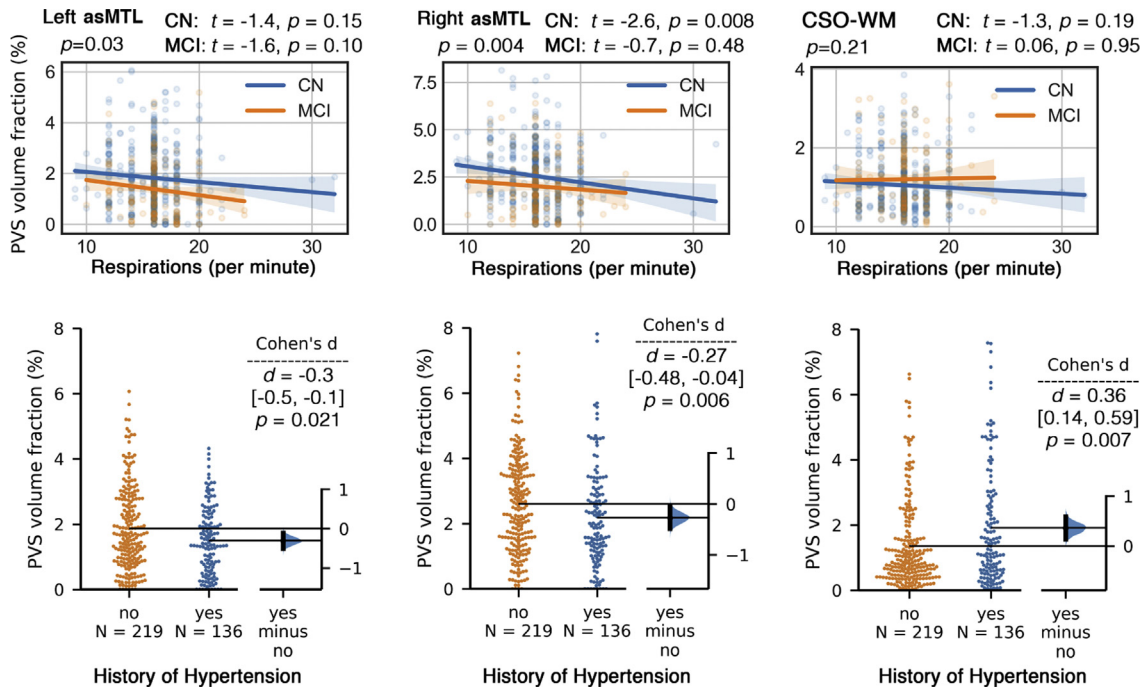


**Fig. 6.** History of hypertension and respiration rate is differentially associated with the PVS volume fraction. First row: Respiratory rate (number of breaths per minute) is negatively associated with PVS volume fraction in asMTL, but not associated with PVS volume fraction in CSO-WM. Second row: Participants with history of hypertension had significantly higher PVS volume fraction in CSO-WM; PVS volume fraction in asMTL was lower in participants with history of hypertension (but not significant after correcting for covariates). Abbreviations: asMTL, anterosuperior medial temporal lobe; CN, cognitively normal; CSO-WM, centrum semi-ovale of the white matter; MCI, mild cognitive impairment; PVS, perivascular space.

2017), but the association with tau deposition was not investigated. Recent studies also demonstrated that pathological phenomena associated with PVS alterations, such as neurovascular dysfunction and BBB breakdown, occur early in AD and independently of A $\beta$  and tau (Montagne et al., 2020; Nation et al., 2019). Therefore, additional studies are required to validate this finding and define the diagnostic role of PVSs for the detection of early pathology leading to cognitive dysfunction.

Pathological changes in the structure and/or function of the cerebral microvasculature have been shown to play a major role in dementia (Bakker et al., 2016; Khachaturian et al., 2019; Malone et al., 2019) and hypertension is a significant risk factor for neurodegenerative disease (Faraco and Iadecola, 2013). In this study, PVS volume fraction was significantly lower in the asMTL and significantly higher in the CSO-WM in patients with a history of hypertension. Previous research on the association between PVS and hypertension shows mixed results: there is evidence that suggests PVS in the CSO-WM increases (Arba et al., 2018; Hurford et al., 2014; Zhang et al., 2016), decreases (Charidimou et al., 2014), or does not change (Potter et al., 2015; Riba-Llena et al., 2016) in the presence of hypertension. Indeed, there is accumulating evidence that the PVS of the basal ganglia, not the CSO-WM, is more strongly associated with vascular risk factors (Troili et al., 2020). The relationship between lower PVS volume fraction in the asMTL and a history of hypertension is therefore inquisitive and may suggest a heterogeneous glymphatic response to cerebrovascular stressors across the white matter. Future studies should aim to disentangle the complex variables that contribute to the overall vascular health of patients.

The PVS becomes visible when enlarged and represents a pathological feature of brain vascular damage that indicates obstruction of the CSF/interstitial fluid flow and impairment of the waste clearance system. It is unclear whether PVS enlargement is a cause or consequence of reduced fluid clearance; however, it is associated with a cascade of neurodegenerative, cerebrovascular, and immunological responses. Dilatation of the PVS may be attributed to impaired arterial pulsatility and reduced arterial elasticity (Hadaczek et al., 2006; Iliff et al., 2013; Kress et al., 2014) and the white matter may be particularly vulnerable to the deleterious effects of impaired cerebrovascular reactivity due to the naturally slower blood flow and fewer capillaries that supply the white matter compared to cortical and subcortical gray matter (Lin et al., 2017; Nonaka et al., 2003). Preclinical evidence in a pericyte-deficient mouse model supports the hypothesis that BBB breakdown leads to extravascular accumulation of blood-derived toxic fibrin deposits, with enlargement of PVS and early white matter damage preceding alterations caused by hypoxia in the cortex (Montagne et al., 2018). Alterations to PVS are also associated with systemic inflammation (Schiltz and Sawchenko, 2003), which affects BBB integrity. Pro-inflammatory cytokines induce inflammatory cells to aggregate around the brain vasculature and degrade the extracellular matrix, resulting in BBB dysfunction and alterations to the brain clearance system (Bechmann et al., 2001; Guillemin and Brew, 2004; Rosenberg, 2017). It has also been proposed that the impairment of the glymphatic flow through PVS enlargement might reduce the clearance of metabolic waste products, including A $\beta$  and tau (Rasmussen et al., 2018), whose deposits could further impair the perivascular drainage, leading to their ulterior accumulation in a “feed-forward” process. Because the signal measured in PVS strictly depends on the CSF signal, it is possible that the lower PVS volume fraction observed in the asMTL of patients with MCI may represent a consequence of an early occlusion and/or obstruction of the PVSs, resulting in loss of CSF signal and decreased detectability of PVS prior to its subsequent dilation.

The diverging relationship between PVS volume fraction and cognitive status within the CSO-WM and asMTL suggests that PVS

alterations in the early stages of cognitive decline may follow heterogeneous trajectories of dysfunction depending on the cerebral area. In fact, PVS and their associated perforating arteries present specific morphological features in different brain regions (notably, basal ganglia and centrum semi-ovale) (Adachi et al., 1998) and therefore their alterations might be caused by multiple types of pathological processes, possibly resulting in different types of clinical and neuroimaging manifestations. It is also possible that the observed association between normal cognitive status and higher asMTL PVS volume reflects the greater amount of compensatory supply to or clearance from the MTL in CN compared to MCI, which might represent a protective mechanism against cognitive impairment. However, whether perivascular flow impairment with reduced clearance is attributed to different pathological phenomena in the asMTL and CSO-WM remains to be explored by future studies.

Although our results suggest that PVS may represent a novel indicator of early pathophysiological processes leading to cognitive impairment, several limitations exist. This study utilizes a cross-sectional design, which limits our ability to attribute observed PVS differences to a pathological origin. Because aging is associated with the dysfunction of the clearance system (Kress et al., 2014), future longitudinal studies that focus on examining the alteration of the PVS as a function of the pathophysiology and cognitive decline are demanded to further validate our findings and to evaluate the efficacy of PVS mapping as a surrogate for brain clearance and vascular health. Another limitation is the potential error in automated segmentation approach, similar to any other automated technique. Here we applied a technique that was developed and validated on Human Connectome Project data, which has higher resolution than ADNI (0.7 mm<sup>3</sup> vs. 1 mm<sup>3</sup>). To address this limitation, we manually assessed 25 randomly selected data and evaluated the accuracy of our methodology. We noted high accuracy of the automated technique, especially when FLAIR data were used to correct the misclassified white matter hyperintensities.

Given the limited sensitivity and specificity of T1w images to vascular presence and integrity, we were not able to examine the mechanisms underlying the observed PVS differences. To ensure that the results we found in asMTL were not confounded by the presence of white matter hyperintensities, which we excluded from the study, we compared voxels that were segmented as white matter hyperintensities in FLAIR images across CN and MCI and found no significant difference ( $p = 0.7$ ). It is also fundamental to consider that the MRI-based PVS analysis strongly relies on the image resolution: higher resolution corresponds to increased PVS detection and improved segmentation (Barisano et al., 2018; Madai et al., 2012; Zong et al., 2016). Small PVSs remain still undetected on MRI or are not discernible from noise. This limitation made it difficult to identify on MRI the submillimeter pathological changes in PVS, which are hypothetically supposed to occur at the very early pre-clinical stages of the disease. It is difficult to separate the vasculature from the PVS itself with the current resolutions and contrasts available with MRI. It is also possible that the observed PVS reductions may be driven by restrictions within the vasculature itself. Recently, it has been shown that the vascular reserve in hippocampus is associated with cognitive performance (Perosa et al., 2020). Finally, quantitative characteristics of the PVS using non-invasive techniques, such as diffusion MRI, could be used to extract submillimeter information (Sepehrband et al., 2019b,c).

## 5. Conclusions

In conclusion, we observed that PVS presence and distribution are different in individuals with MCI compared to healthy controls.

Our results demonstrate in vivo that PVS volume fraction of the CSO-WM is higher in MCI compared to CN, and that this difference is mostly found in females. Moreover, we showed that PVS volume fraction is significantly lower within the asMTL of patients with MCI compared to CN, and the lower PVS content in this region was associated with higher aggregation of tau neurofibrillary tangles. Together, these results suggest that PVS alterations in the asMTL may represent an early feature of AD pathology. This discovery encourages further investigation of the cerebral PVS in terms of pathophysiology, diagnostic role, and new potential therapeutic strategies for cognitive dysfunction.

#### Disclosure statement

The authors have no conflict of interest to declare.

#### CRedit authorship contribution statement

**Farshid Sepehrband:** Conceptualization, Methodology, Data curation, Validation, Formal analysis, Writing - original draft, Visualization, Supervision. **Giuseppe Barisano:** Conceptualization, Methodology, Formal analysis, Writing - original draft. **Nasim Sheikh-Bahaei:** Conceptualization, Writing - review & editing, Validation. **Jeiran Choupan:** Methodology, Data curation, Writing - review & editing. **Ryan P. Cabeen:** Methodology, Writing - review & editing. **Kirsten M. Lynch:** Writing - original draft, Validation. **Malcolm S. Crawford:** Conceptualization, Writing - review & editing. **Haoyu Lan:** Methodology, Writing - review & editing. **Wendy J. Mack:** Methodology, Writing - review & editing. **Helena C. Chui:** Conceptualization, Supervision, Funding acquisition. **John M. Ringman:** Conceptualization, Validation, Conceptualization, Supervision, Funding acquisition.

#### Acknowledgements

This work was supported by NIH grants: 2P41EB015922-21, 1P01AG052350-01 and USC ADRC 5P50AG005142 and 1P30AG066530-01. This research reported in this publication was also supported by the National Institute of Mental Health of the NIH under Award Number RF1MH123223. The content is solely the responsibility of the authors and does not necessarily represent the official views of the NIH. **ADNI:** Data collection and sharing for this project was funded by the Alzheimer's Disease Neuroimaging Initiative (ADNI) (National Institutes of Health Grant U01 AG024904) and DOD ADNI (Department of Defense award number W81XWH-12-2-0012). ADNI is funded by the National Institute on Aging, the National Institute of Biomedical Imaging and Bioengineering, and through generous contributions from the following: AbbVie, Alzheimer's Association; Alzheimer's Drug Discovery Foundation; Araclon Biotech; BioClinica, Inc.; Biogen; Bristol-Myers Squibb Company; CereSpir, Inc.; Cogstate; Eisai Inc.; Elan Pharmaceuticals, Inc.; Eli Lilly and Company; EuroImmun; F. Hoffmann-La Roche Ltd and its affiliated company Genentech, Inc.; Fujirebio; GE Healthcare; IXICO Ltd.; Janssen Alzheimer Immunotherapy Research & Development, LLC.; Johnson & Johnson Pharmaceutical Research & Development LLC.; Lumosity; Lundbeck; Merck & Co., Inc.; Meso Scale Diagnostics, LLC.; NeuroRx Research; Neurotrack Technologies; Novartis Pharmaceuticals Corporation; Pfizer Inc.; Piramal Imaging; Servier; Takeda Pharmaceutical Company; and Transition Therapeutics. The Canadian Institutes of Health Research is providing funds to support ADNI clinical sites in Canada. Private sector contributions are facilitated by the Foundation for the National Institutes of Health ([www.fnih.org](http://www.fnih.org)). The grantee organization is the Northern California Institute for Research and Education, and the study is coordinated by the Alzheimer's Therapeutic Research

Institute at the University of Southern California. ADNI data are disseminated by the Laboratory for Neuro Imaging at the University of Southern California.

#### Appendix A. Supplementary data

Supplementary data to this article can be found online at <https://doi.org/10.1016/j.neurobiolaging.2020.12.010>.

#### References

- Adachi, M., Hosoya, T., Haku, T., Yamaguchi, K., 1998. Dilated Virchow-Robin spaces: MRI pathological study. *Neuroradiology* 40, 27–31.
- Arba, F., Quinn, T.J., Hankey, G.J., Lees, K.R., Wardlaw, J.M., Ali, M., 2018. Enlarged perivascular spaces and cognitive impairment after stroke and transient ischemic attack. *Int. J. Stroke* 13, 47–56.
- Avants, B.B., Tustison, N., Song, G., 2009. Advanced Normalization Tools (ANTS). *Insight J.* 2, 1–35.
- Avants, B.B., Tustison, N.J., Song, G., Cook, P.A., Klein, A., Gee, J.C., 2011. A reproducible evaluation of ANTs similarity metric performance in brain image registration. *Neuroimage* 54, 2033–2044.
- Baker, S.L., Lockhart, S.N., Price, J.C., He, M., Huesman, R.H., Schonhaut, D., Faria, J., Rabinovici, G., Jagust, W.J., 2017a. Reference tissue-based kinetic evaluation of 18F-AV-1451 for tau imaging. *J. Nucl. Med.* 58, 332–338.
- Baker, S.L., Maass, A., Jagust, W.J., 2017b. Considerations and code for partial volume correcting [(18)F]-AV-1451 tau PET data. *Data Br.* 15, 648–657.
- Bakker, E.N.T.P., Bacskai, B.J., Arbel-Ornath, M., Aldea, R., Bedussi, B., Morris, A.W.J., Weller, R.O., Carare, R.O., 2016. Lymphatic clearance of the brain: perivascular, paravascular and significance neurodegenerative diseases. *Cell. Mol. Neurobiol.* 36, 181–194.
- Banerjee, G., Kim, H.J., Fox, Z., Jager, H.R., Wilson, D., Charidimou, A., Na, H.K., Na, D.L., Seo, S.W., Werring, D.J., 2017. MRI-visible perivascular space location is associated with Alzheimer's disease independently of amyloid burden. *Brain* 140, 1107–1116.
- Barisano, G., Sepehrband, F., Ma, S., Jann, K., Cabeen, R., Wang, D.J., Toga, A.W., Law, M., 2018. Clinical 7 T MRI: are we there yet? A review about magnetic resonance imaging at ultra-high field. *Br. J. Radiol.* 91, 20180492.
- Battisti-Charbonney, A., Fisher, J., Duffin, J., 2011. The cerebrovascular response to carbon dioxide in humans. *J. Physiol.* 589, 3039–3048.
- Beak, H.W., Choi, H.J., Byun, M.S., Choe, Y.M., Yi, D., Han, J.Y., Lee, Y.J., Woo, J.I., Lee, D.Y., 2015. Prevalence of enlarged perivascular spaces in a memory clinic population. *Alzheimer's Dement. J. Alzheimer's Assoc.* 11, P146.
- Bechmann, I., Priller, J., Kovac, A., Bontert, M., Wenhner, T., Klett, F.F., Bechmann, I., Priller, J., Kovac, A., Bo, M., Stuschke, M., Dirnagl, U., Nitsch, R., 2001. Immune surveillance of mouse brain perivascular spaces by blood-borne macrophages. *Eur. J. Neurosci.* 14, 1651–1658.
- Bennett, M., Cantini, M., Reboud, J., Cooper, J.M., Roca-Cusachs, P., Salmeron-Sanchez, M., 2018. Molecular clutch drives cell response to surface viscosity. *Proc. Natl. Acad. Sci. U. S. A.* 115, 1192–1197.
- Blair, L.J., Frauen, H.D., Zhang, B., Nordhues, B.A., Bijan, S., Lin, Y.-C., Zamudio, F., Hernandez, L.D., Sabbagh, J.J., Selenica, M.-L.B., Dickey, C.A., 2015. Tau depletion prevents progressive blood-brain barrier damage in a mouse model of tauopathy. *Acta Neuropathol. Commun.* 3, 1–22.
- Braak, H., Braak, E., 1991. Neuropathological staging of Alzheimer-related changes. *Acta Neuropathol.* 82, 239–259.
- Braak, H., Braak, E., 1996. Evolution of the neuropathology of Alzheimer's disease. *Acta Neurol. Scand.* 94, 3–12.
- Brendel, M., Högenauer, M., Delker, A., Sauerbeck, J., Bartenstein, P., Seibyl, J., Rominger, A., 2015. Improved longitudinal [18F]-AV45 amyloid PET by white matter reference and VOI-based partial volume effect correction. *Neuroimage* 108, 450–459.
- Cabeen, R.P., Laidlaw, D.H., Toga, A.W., 2018. Quantitative imaging toolkit: software for interactive 3D visualization, data exploration, and computational analysis of neuroimaging datasets. *ISMRM-ESMRMB Abstr.* 2854, 12–14.
- Carare, R.O., Bernardes-Silva, M., Newman, T.A., Page, A.M., Nicoll, J.A.R., Perry, V.H., Weller, R.O., 2008. Solutes, but not cells, drain from the brain parenchyma along basement membranes of capillaries and arteries: significance for cerebral amyloid angiopathy and neuroimmunology. *Neuropathol. Appl. Neurobiol.* 34, 131–144.
- Charidimou, A., Boulouis, G., Pasi, M., Etten, E.S., Van, Haley, K., Ayres, A., Schwab, K.M., Greenberg, S.M., 2017. MRI-visible perivascular spaces in cerebral amyloid angiopathy and hypertensive arteriopathy. *Am. Acad. Neurol.* 88, 1157–1164.
- Charidimou, A., Hong, Y.T., Jäger, H.R., Fox, Z., Aigbirhio, F.I., Fryer, T.D., Menon, D.K., Warburton, E.A., Werring, D.J., Baron, J., 2015. White matter perivascular spaces on magnetic resonance imaging—marker of cerebrovascular amyloid burden? *Stroke* 46, 1707–1709.
- Charidimou, A., Jäger, R.H., Peeters, A., Vandermeeren, Y., Laloux, P., Baron, J., Werring, D.J., 2014. White matter perivascular spaces are related to cortical superficial siderosis in cerebral amyloid angiopathy. *Stroke* 45, 2930–2935.

- Charidimou, A., Meegahage, R., Fox, Z., Peeters, A., Vandermeeren, Y., Laloux, P., Baron, J.-C., Jäger, H.R., Werring, D.J., 2013. Enlarged perivascular spaces as a marker of underlying arteriopathy in intracerebral haemorrhage: a multicentre MRI cohort study. *J. Neurol. Neurosurg. Psychiatry* 84, 624–629.
- Chen, K., Rontiva, A., Thiyyagura, P., Lee, W., Liu, X., Ayutyanont, N., Protas, H., Luo, J.L., Bauer, R., Reschke, C., Bandy, D., Koeppe, R.A., Fleisher, A.S., Caselli, R.J., Landau, S., Jagust, W.J., Weiner, M.W., Reiman, E.M., 2015. Improved power for characterizing longitudinal amyloid-PET changes and evaluating amyloid-modifying treatments with a cerebral white matter reference region. *J. Nucl. Med.* 56, 560–566.
- Chen, W., Song, X., Zhang, Y., 2011. Assessment of the Virchow-Robin spaces in Alzheimer disease, mild cognitive impairment, and normal aging, using high-field MR imaging. *AJNR* 32, 1490–1495.
- Clark, C.M., Schneider, J.A., Bedell, B.J., Beach, T.G., Bilker, W.B., Mintun, M.A., Pontecorvo, M.J., Hefti, F., Carpenter, A.P., Flitter, M.L., Krautkramer, M.J., Kung, H.F., Coleman, R.E., Doraiswamy, P.M., Fleisher, A.S., Sabbagh, M.N., Sadowsky, C.H., Reiman, E.P., Zehntner, S.P., Skovronsky, D.M., Group, A.-A.S., 2011. Use of florbetapir-PET for imaging beta-amyloid pathology. *JAMA* 305, 275–283.
- Corder, E.H., Saunders, A.M., Strittmatter, W.J., Schmechel, D.E., Gaskell, P.C., Small, G.W., Roses, A.D., Haines, J.L., Pericak-Vance, M.A., 1993. Gene dose of apolipoprotein E type 4 allele and the risk of Alzheimer's disease in late onset families. *Science* 261, 921–923.
- Da Mesquita, S., Louveau, A., Vaccari, A., Smirnov, I., Cornelison, R.C., Kingsmore, K.M., Contarino, C., Onengut-Gumuscu, S., Farber, E., Raper, D., 2018. Functional aspects of meningeal lymphatics in ageing and Alzheimer's disease. *Nature* 560, 185–191.
- Dale, A., Fischl, B., Sereno, M.I., 1999. Cortical surface-based analysis: I. Segmentation and surface reconstruction. *Neuroimage* 9, 179–194.
- De Long, W.B., 1973. Anatomy of the middle cerebral artery: the temporal branches. *Stroke* 4, 412–418.
- Desikan, R.S., Ségonne, F., Fischl, B., Quinn, B.T., Dickerson, B.C., Blacker, D., Buckner, R.L., Dale, A.M., Maguire, R.P., Hyman, B.T., Albert, M.S., Killiany, R.J., 2006. An automated labeling system for subdividing the human cerebral cortex on MRI scans into gyral based regions of interest. *Neuroimage* 31, 968–980.
- Diedrichsen, J., 2006. A spatially unbiased atlas template of the human cerebellum. *Neuroimage* 33, 127–138.
- Diem, A.K., MacGregor Sharp, M., Gatherer, M., Bressloff, N.W., Carare, R.O., Richardson, G., 2017. Arterial pulsations cannot drive intramural periarterial drainage: significance for Aβ drainage. *Front. Neurosci.* 11, 1–9.
- Dinov, I., Lozev, K., Petrosyan, P., Liu, Z., Eggert, P., 2010. Neuroimaging study designs, computational analyses and data provenance using the LONI pipeline. *PLoS One* 5, e13070.
- Dinov, I.D., Van Horn, J.D., Lozev, K.M., Magsipoc, R., Petrosyan, P., Liu, Z., MacKenzie-Graham, A., Eggert, P., Parker, D.S., Toga, A.W., 2009. Efficient, distributed and interactive neuroimaging data analysis using the LONI pipeline. *Front. Neuroinform.* 3, 22.
- Doubal, F.N., MacLulich, A.M.J., Ferguson, K.J., Dennis, M.S., Wardlaw, J.M., 2010. Enlarged perivascular spaces on MRI are a feature of cerebral small vessel disease. *Stroke* 41, 450–454.
- Faraco, G., Iadecola, C., 2013. Hypertension: a harbinger of stroke and dementia. *Hypertension* 62, 810–817.
- Ferguson, S.C., Blane, A., Perros, P., McCrimmon, R.J., Best, J.J.K., Wardlaw, J., Deary, I.J., Frier, B.M., 2003. Cognitive ability and brain structure in type 1 diabetes: relation to microangiopathy and preceding severe hypoglycemia. *Diabetes* 52, 149–156.
- Fischl, B., 2012. FreeSurfer. *Neuroimage* 62, 774–781.
- Fischl, B., Dale, A.M., 2000. Measuring the thickness of the human cerebral cortex from magnetic resonance images. *Proc. Natl. Acad. Sci.* 97, 11050–11055.
- Fischl, B., Salat, D.H., Busa, E., Albert, M., Dieterich, M., Haselgrove, C., Van Der Kouwe, A., Killiany, R., Kennedy, D., Klaveness, S., 2002. Whole brain segmentation: automated labeling of neuroanatomical structures in the human brain. *Neuron* 33, 341–355.
- Fischl, B., Salat, D.H., van der Kouwe, A.J.W., Makris, N., Ségonne, F., Quinn, B.T., Dale, A.M., 2004a. Sequence-independent segmentation of magnetic resonance images. *Neuroimage* 23, S69–S84.
- Fischl, B., Sereno, M.I., Dale, A., 1999. Cortical surface-based analysis: II: inflation, flattening, and a surface-based coordinate system. *Neuroimage* 9, 195–207.
- Fischl, B., van der Kouwe, A., Destrieux, C., Halgren, E., Ségonne, F., Salat, D.H., Busa, E., Seidman, L.J., Goldstein, J., Kennedy, D., Caviness, V., Makris, N., Rosen, B., Dale, A.M., 2004b. Automatically parcellating the human cerebral cortex. *Cereb. Cortex* 14, 11–22.
- Folstein, M.F., Robins, L.N., Helzer, J.E., 1983. The mini-mental state examination. *Arch. Gen. Psychiatry* 40, 812.
- Francis, F., Ballerini, L., Wardlaw, J.M., 2019. Perivascular spaces and their associations with risk factors, clinical disorders and neuroimaging features: a systematic review and meta-analysis. *Int. J. Stroke* 14, 359–371.
- Frangi, A.F., Niessen, W.J., Vincken, K.L., Viergever, M.A., 1998. Multiscale vessel enhancement filtering, in: International Conference on Medical Image Computing and Computer-Assisted Intervention. Springer 130–137.
- Guillemin, G.J., Brew, B.J., 2004. Microglia, macrophages, perivascular macrophages, and pericytes: a review of function and identification. *J. Leukoc. Biol.* 75, 388–397.
- Hadaczek, P., Yamashita, Y., Mirek, H., Tamas, L., Bohn, M.C., Noble, C., Park, J.W., Bankiewicz, K., 2006. The “perivascular pump” driven by arterial pulsation is a powerful mechanism for the distribution of therapeutic molecules within the brain. *Mol. Ther.* 14, 69–78.
- Hilal, S., Tan, C.S., Adams, H.H.H., Habes, M., Mok, V., Venketasubramanian, N., Hofer, E., Ikram, M.K., Abrego, J., Vernooij, M.W., Chen, C., Hosten, N., Volzke, H., Grabe, H.J., Schmidt, R., Ikram, M.A., 2018. Enlarged perivascular spaces and cognition: a meta-analysis of 5 population-based studies. *Neurology* 91, e832–e842.
- Ho, J., Tumkaya, T., Aryal, S., Choi, H., Claridge-Chang, A., 2019. Moving beyond P values: data analysis with estimation graphics. *Nat. Methods* 16, 565–566.
- Hughes, C.P., Berg, L., Danziger, W.L., Coben, L.A., Martin, R.L., 1982. A new clinical scale for the staging of dementia. *Br. J. Psychiatry* 140, 566–572.
- Hurford, R., Charidimou, A., Fox, Z., Cicolotti, L., Jager, R., Werring, D.J., 2014. MRI-visible perivascular spaces: relationship to cognition and small vessel disease MRI markers in ischaemic stroke and TIA. *J. Neurol. Neurosurg. Psychiatry* 85, 522–525.
- Iadecola, C., 2017. The neurovascular unit coming of age: a journey through neurovascular coupling in health and disease. *Neuron* 96, 17–42.
- Iliff, J.J., Nedergaard, M., 2013. Is there a cerebral lymphatic system? *Stroke* 44, S93–S95.
- Iliff, J.J., Wang, M., Liao, Y., Plogg, B.A., Peng, W., Gundersen, G.A., Benveniste, H., Vates, G.E., Deane, R., Goldman, S.A., Nagelhus, E.A., Nedergaard, M., 2012. A paravascular pathway facilitates CSF flow through the brain parenchyma and the clearance of interstitial solutes, including amyloid β. *Sci. Transl. Med.* 4, 1–11.
- Iliff, J.J., Wang, M., Zeppenfeld, D.M., Venkataraman, A., Plog, B.A., Liao, Y., Deane, R., Nedergaard, M., 2013. Cerebral arterial pulsation drives paravascular CSF-interstitial fluid exchange in the murine brain. *J. Neurosci.* 33, 18190–18199.
- Ishikawa, M., Yamada, S., Yamamoto, K., 2018. Dilated perivascular spaces in the centrum semiovale begin to develop in middle age. *J. Alzheimer's Dis.* 61, 1619–1626.
- Jagust, W.J., Landau, S.M., Shaw, L.M., Trojanowski, J.Q., Koeppe, R.A., Reiman, E.M., Foster, N.L., Petersen, R.C., Weiner, M.W., Price, J.C., Mathis, C.A., Initiative, A.D.N., 2009. Relationships between biomarkers in aging and dementia. *Neurology* 73, 1193–1199.
- Jeong, E.H., Lee, Y.J., Kim, S.J., Lee, J.-H., 2015. Is the severity of dilated Virchow-Robin spaces associated with cognitive dysfunction? *Dement. Neurocognitive Disord.* 14, 114–119.
- Jiménez-Balado, J., Riba-Llena, I., Garde, E., Valor, M., Gutiérrez, B., Pujadas, F., Delgado, P., 2018. Prevalence of hippocampal enlarged perivascular spaces in a sample of patients with hypertension and their relation with vascular risk factors and cognitive function. *J. Neurol. Neurosurg. Psychiatry* 89, 651–656.
- Joshi, A.D., Pontecorvo, M.J., Clark, C.M., Carpenter, A.P., Jennings, D.L., Sadowsky, C.H., Adler, L.P., Kovnat, K.D., Seibyl, J.P., Arora, A., Saha, K., Burns, J.D., Lowrey, M.J., Mintun, M.A., Skovronsky, D.M., 2012. Performance characteristics of amyloid PET with florbetapir F 18 in patients with Alzheimer's disease and cognitively normal subjects. *J. Nucl. Med.* 53, 378–384.
- Kalaria, R.N., Ballard, C., 1999. Overlap between pathology of Alzheimer disease and vascular dementia. *Alzheimer Dis. Assoc. Disord.*
- Kang, J.-H., Korecka, M., Figurski, M.J., Toledo, J.B., Blennow, K., Zetterberg, H., Waligorska, T., Brylka, M., Fields, L., Shah, N., 2015. The Alzheimer's disease neuroimaging initiative 2 biomarker core: a review of progress and plans. *Alzheimer's Dement.* 11, 772–791.
- Kepe, V., 2013. Amyloid PET imaging. *PET. Clin.* 8, 431–445.
- Khachaturian, Z.S., Kuller, L.H., Khachaturian, A.S., 2019. Strategic goals and roadmap for dementia prevention by stroke prevention. *Alzheimer's Dement.* 15, 865–869.
- Kisler, K., Nelson, A.R., Montagne, A., Zlokovic, B.V., 2017. Cerebral blood flow regulation and neurovascular dysfunction in Alzheimer disease. *Nat. Rev. Neurosci.* 18, 419–434.
- Klarenbeek, P., van Oostenbrugge, R.J., Lodder, J., Rouhl, R.P.W., Knottnerus, I.L.H., Staals, J., 2013. Higher ambulatory blood pressure relates to enlarged Virchow-Robin spaces in first-ever lacunar stroke patients. *J. Neurol.* 260, 115–121.
- Korecka, M., Waligorska, T., Figurski, M., Toledo, J.B., Arnold, S.E., Grossman, M., Trojanowski, J.Q., Shaw, L.M., 2014. Qualification of a surrogate matrix-based absolute quantification method for amyloid-β 42 in human cerebrospinal fluid using 2D UPLC-tandem mass spectrometry. *J. Alzheimer's Dis.* 41, 441–451.
- Kress, B.T., Iliff, J.J., Xia, M., Wang, M., Wei, H.S., Zeppenfeld, D., Xie, L., Kang, H., Xu, Q., Liew, J.A., 2014. Impairment of paravascular clearance pathways in the aging brain. *Ann. Neurol.* 76, 845–861.
- Landau, S.M., Breault, C., Joshi, A.D., Pontecorvo, M., Mathis, C.A., Jagust, W.J., Mintun, M.A., Initiative, A.D.N., 2013a. Amyloid-β imaging with Pittsburgh compound B and florbetapir: comparing radiotracers and quantification methods. *J. Nucl. Med.* 54, 70–77.
- Landau, S.M., Fero, A., Baker, S.L., Koeppe, R., Mintun, M., Chen, K., Reiman, E.M., Jagust, W.J., 2015. Measurement of longitudinal β-amyloid change with 18F-florbetapir PET and standardized uptake value ratios. *J. Nucl. Med.* 56, 567–574.
- Landau, S.M., Lu, M., Joshi, A.D., Pontecorvo, M., Mintun, M.A., Trojanowski, J.Q., Shaw, L.M., Jagust, W.J., Initiative, A.D.N., 2013b. Comparing positron emission tomography imaging and cerebrospinal fluid measurements of β-amyloid. *Ann. Neurol.* 74, 826–836.
- Landau, S.M., Mintun, M.A., Joshi, A.D., Koeppe, R.A., Petersen, R.C., Aisen, P.S., Weiner, M.W., Jagust, W.J., Initiative, A.D.N., 2012. Amyloid deposition, hypometabolism, and longitudinal cognitive decline. *Ann. Neurol.* 72, 578–586.
- Landau, S.M., Thomas, B.A., Thurfjell, L., Schmidt, M., Margolin, R., Mintun, M., Pontecorvo, M., Baker, S.L., Jagust, W.J., Initiative, A.D.N., 2014. Amyloid PET

- imaging in Alzheimer's disease: a comparison of three radiotracers. *Eur. J. Nucl. Med. Mol. Imaging* 41, 1398–1407.
- Lin, J., Wang, D., Lan, L., Fan, Y., 2017. Multiple factors involved in the pathogenesis of white matter lesions. *Biomed. Res. Int.* 2017.
- Louveau, A., Herz, J., Alme, M.N., Salvador, A.F., Dong, M.Q., Viar, K.E., Herod, S.G., Knopp, J., Setliff, J.C., Lupi, A.L., 2018. CNS lymphatic drainage and neuroinflammation are regulated by meningeal lymphatic vasculature. *Nat. Neurosci.* 21, 1380–1391.
- Maass, A., Landau, S., Horng, A., Lockhart, S.N., Rabinovici, G.D., Jagust, W.J., Baker, S.L., La Joie, R., 2017. Comparison of multiple tau-PET measures as biomarkers in aging and Alzheimer's disease. *Neuroimage* 157, 448–463.
- MacLulich, A.M.J., Wardlaw, J.M., Ferguson, K.J., Starr, J.M., Seckl, J.R., Deary, I.J., 2004. Enlarged perivascular spaces are associated with cognitive function in healthy elderly men. *J. Neurol. Neurosurg. Psychiatry* 75, 1519–1523.
- Madaï, V.I., von Samson-Himmelstjerna, F.C., Bauer, M., Stengl, K.L., Mutke, M.A., Tovar-Martinez, E., Wuerfel, J., Endres, M., Niendorf, T., Sobesky, J., 2012. Ultrahigh-field MRI in human ischemic stroke—a 7 Tesla study. *PLoS One* 7, e37631.
- Malone, K., Amu, S., Moore, A.C., Waeber, C., 2019. The immune system and stroke: from current targets to future therapy. *Immunol. Cell Biol.* 97, 5–16.
- Manjón, J.V., Coupé, P., Martí-Bonmati, L., Collins, D.L., Robles, M., 2010. Adaptive non-local means denoising of MR images with spatially varying noise levels. *J. Magn. Reson. Imaging* 31, 192–203.
- Marchi, N., Banjar, M., Janigro, D., 2016. Blood–brain barrier, bulk flow, and interstitial clearance in epilepsy. *J. Neurosci. Methods* 34, 352–359.
- Montagne, A., Nation, D.A., Sagare, A.P., Barisano, G., Sweeney, M.D., Chakhoyan, A., Pachicano, M., Joe, E., Nelson, A.R., D'Orazio, L.M., 2020. APOE4 leads to blood–brain barrier dysfunction predicting cognitive decline. *Nature* 581, 71–76.
- Montagne, A., Nikolakopoulou, A.M., Zhao, Z., Sagare, A.P., Si, G., Lasic, D., Barnes, S.R., Daianu, M., Ramanathan, A., Go, A., Lawson, E.J., Wang, Y., Mack, W.J., Thompson, P.M., Schneider, J.A., Varkey, J., Langen, R., Mullins, E., Jacobs, R.E., Zlokovic, B., V., 2018. Pericyte degeneration causes white matter dysfunction in the mouse central nervous system. *Nat. Med.* 24, 326.
- Moon, S.W., Dinov, I.D., Kim, J., Zamanyan, A., Hobel, S., Thompson, P.M., Toga, A.W., 2015. Structural neuroimaging genetics interactions in Alzheimer's disease. *J. Alzheimer's Dis.* 48, 1051–1063.
- Mormino, E.C., Kluth, J.T., Madison, C.M., Rabinovici, G.D., Baker, S.L., Miller, B.L., Koeppe, R.A., Mathis, C.A., Weiner, M.W., Jagust, W.J., Initiative, A.D.N., 2009. Episodic memory loss is related to hippocampal-mediated beta-amyloid deposition in elderly subjects. *Brain* 132, 1310–1323.
- Morris, J.C., 1993. The clinical dementia rating (cdr): current version and scoring rules. *Neurology* 43, 2412–2414.
- Nation, Daniel A., Sweeney, M.D., Montagne, A., Sagare, A.P., D'Orazio, L.M., Pachicano, M., Sepehrband, F., Nelson, A.R., Buennagel, D.P., Harrington, M.G., Benzinger, T.L.S., Fagan, A.M., Ringman, J.M., Schneider, L.S., Morris, J.C., Chui, H.C., Law, M., Toga, A.W., Zlokovic, B.V., 2019. Blood–brain barrier breakdown is an early biomarker of human cognitive dysfunction. *Nat. Med.* 25, 270–276.
- Nedergaard, M., 2013. Garbage truck of the brain. *Science* (80-. ) 340, 1529–1530.
- Nonaka, H., Akima, M., Hatori, T., Nagayama, T., Zhang, Z., Ihara, F., 2003. The microvasculature of the cerebral white matter: arteries of the subcortical white matter. *J. Neuropathol. Exp. Neurol.* 62, 154–161.
- Panza, F., Solfrizzi, V., Torres, F., Mastroianni, F., Colacicco, A.M., Basile, A.M., Capurso, C., D'Introno, A., Del Parigi, A., Capurso, A., 2000. Apolipoprotein E in Southern Italy: protective effect of  $\epsilon 2$  allele in early- and late-onset sporadic Alzheimer's disease. *Neurosci. Lett.* 292, 79–82.
- Park, L., Uekawa, K., Garcia-Bonilla, L., Koizumi, K., Murphy, M., Pistik, R., Younkin, L., Younkin, S., Zhou, P., Carlson, G., Anrather, J., Iadecola, C., 2017. Brain perivascular macrophages initiate the neurovascular dysfunction of Alzheimer abeta peptides. *Circ. Res.* 121, 258–269.
- Passiak, B.S., Liu, D., Kresge, H.A., Cambronero, F.E., Pechman, K.R., Osborn, K.E., Gifford, K.A., Hohman, T.J., Schrag, M.S., Davis, L.T., 2019. Perivascular spaces contribute to cognition beyond other small vessel disease markers. *Neurology* 92, e1309–e1321.
- Pearson, E.S., D'agostino, R.B., Bowman, K.O., 1977. Tests for departure from normality: comparison of powers. *Biometrika* 64, 231–246.
- Perlmutter, J.S., Powers, W.J., Herscovitch, P., Fox, P.T., Raichle, M.E., 1987. Regional asymmetries of cerebral blood flow, blood volume, and oxygen utilization and extraction in normal subjects. *J. Cereb. Blood Flow Metab.* 7, 64–67.
- Perosa, V., Priester, A., Ziegler, G., Cardenas-Blanco, A., Dobisch, L., Spallazzi, M., Assmann, A., Maass, A., Speck, O., Oltmer, J., Heinze, H.J., Schreiber, S., Düzél, E., 2020. Hippocampal vascular reserve associated with cognitive performance and hippocampal volume. *Brain* 143, 622–634.
- Potter, G.M., Doubal, F.N., Jackson, C.A., Chappell, F.M., Sudlow, C.L., Dennis, M.S., Wardlaw, J.M., 2015. Enlarged perivascular spaces and cerebral small vessel disease. *Int. J. Stroke* 10, 376–381.
- Qiu, C., Kivipelto, M., Agüero-Torres, H., Winblad, B., Fratiglioni, L., 2004. Risk and protective effects of the APOE gene towards Alzheimer's disease in the Kungsholmen project: variation by age and sex. *J. Neurol. Neurosurg. Psychiatry* 75, 828–833.
- Ramirez, J., Berezuk, C., McNeely, A.A., Gao, F., McLaurin, J., Black, S.E., 2016. Imaging the perivascular space as a potential biomarker of neurovascular and neurodegenerative diseases. *Cell. Mol. Neurobiol.* 36, 289–299.
- Ramirez, J., Berezuk, C., McNeely, A.A., Scott, C.J.M., Gao, F., Black, S.E., 2015. Visible Virchow-Robin spaces on magnetic resonance imaging of Alzheimer's disease patients and normal elderly from the Sunnybrook dementia study. *J. Alzheimer's Dis.* 43, 415–424.
- Rasmussen, M.K., Mestre, H., Nedergaard, M., 2018. The glymphatic pathway in neurological disorders. *Lancet Neurol.* 17, 1016–1024.
- Reilhac, A., Rousset, O.G., Comtat, C., Frouin, V., Gregoire, M.-C., Evans, A.C., 2000. A Correction Algorithm Partial Volume Effects 3d PET. *Imaging: Principle Validation. IEEE Nucl. Sci. Symp. Conf. Rec. (Cat. No.00CH37149).*
- Reuter, M., Fischl, B., 2011. Avoiding asymmetry-induced bias in longitudinal image processing. *Neuroimage* 57, 19–21.
- Reuter, M., Rosas, H.D., Fischl, B., 2010. Highly accurate inverse consistent registration: a robust approach. *Neuroimage* 53, 1181–1196.
- Reuter, M., Schmansky, N.J., Rosas, H.D., Fischl, B., 2012. Within-subject template estimation for unbiased longitudinal image analysis. *Neuroimage* 61, 1402–1418.
- Riba-Llena, I., Nafria, C., Mundet, X., Lopez-Rueda, A., Fernandez-Cortinas, I., Jarca, C.I., Jimenez-Balado, J., Domingo, M., Tovar, J.L., Orfila, F., Pujadas, F., Alvarez-Sabin, J., Maisterra, O., Montaner, J., Delgado, P., 2016. Assessment of enlarged perivascular spaces and their relation to target organ damage and mild cognitive impairment in patients with hypertension. *Eur. J. Neurol.* 23, 1044–1050.
- Rosenberg, G.A., 2017. Extracellular matrix inflammation in vascular cognitive impairment and dementia. *Clin. Sci.* 131, 425–437.
- Rouhl, R.P.W., Van Oostenbrugge, R.J., Knottnerus, I.L.H., Staals, J.E.A., Lodder, J., 2008. Virchow-Robin spaces relate to cerebral small vessel disease severity. *J. Neurol.* 255, 692–696.
- Schiltz, J.C., Sawchenko, P.E., 2003. Signaling the brain in systemic inflammation: the role of perivascular cells. *Front. Biosci.* 8, s1321–s1329.
- Schöll, M., Lockhart, S.N., Schonhaut, D.R., O'Neil, J.P., Janabi, M., Ossenkoppele, R., Baker, S.L., Vogel, J.W., Faria, J., Schwimmer, H.D., 2016. PET imaging of tau deposition in the aging human brain. *Neuron* 89, 971–982.
- Segonne, F., Dale, A.M., Busa, E., Glessner, M., Salat, D., Hahn, H.K., Fischl, B., 2004. A hybrid approach to the skull stripping problem in MRI. *Neuroimage* 22, 1060–1075.
- Segonne, F., Pacheco, J., Fischl, B., 2007. Geometrically accurate topology-correction of cortical surfaces using nonseparating loops. *IEEE Trans. Med. Imaging* 26, 518–529.
- Sepehrband, F., Barisano, G., Sheikh-Bahaei, N., Cabeen, R.P., Choupan, J., Law, M., Toga, A.W., 2019a. Image processing approaches to enhance perivascular space visibility and quantification using MRI. *Sci. Rep.* 9, 1–12.
- Sepehrband, F., Cabeen, R.P., Barisano, G., Sheikh-Bahaei, N., Choupan, J., Law, M., Toga, A.W., 2019b. Nonparenchymal fluid is the source of increased mean diffusivity in preclinical Alzheimer's disease. *Alzheimer's Dement. Diagnosis, Assess. Dis. Monit.* 11, 348–354.
- Sepehrband, F., Cabeen, R.P., Choupan, J., Barisano, G., Law, M., Toga, A.W., 2019c. Perivascular space fluid contributes to diffusion tensor imaging changes in white matter. *Neuroimage* 197, 243–254.
- Sepehrband, F., Lynch, K.M., Cabeen, R.P., Gonzalez-Zacarias, C., Zhao, L., D'Arcy, M., Kesselman, C., Herting, M.M., Dinov, I.D., Toga, A.W., Clark, K.A., 2018. Neuro-anatomical morphometric characterization of sex differences in youth using statistical learning. *Neuroimage* 172, 217–227.
- Sled, J.G., Zijdenbos, A.P., Evans, A.C., 1998. A nonparametric method for automatic correction of intensity nonuniformity in MRI data. *IEEE Trans. Med. Imaging* 17, 87–97.
- Sta Cruz, S., Dinov, I.D., Herting, M.M., Gonzalez-Zacarias, C., Kim, H., Toga, A.W., Sepehrband, F., 2019. Imputation strategy for reliable regional MRI morphological measurements. *Neuroinformatics* 18, 59–70.
- Sweeney, M.D., Sagare, A.P., Zlokovic, B., V., 2018. Blood–brain barrier breakdown in Alzheimer disease and other neurodegenerative disorders. *Nat. Rev. Neurol.* 14, 133.
- Thomas, T., Thomas, G., McLendon, C., Sutton, T., Mullan, M., 1996.  $\beta$ -Amyloid-mediated vasoactivity and vascular endothelial damage. *Nature* 380, 168.
- Toga, A.W., Crawford, K.L., 2010. The informatics core of the Alzheimer's Disease Neuroimaging Initiative. *Alzheimer's Dement* 6, 247–256.
- Torri, F., Dinov, I.D., Zamanyan, A., Hobel, S., Genco, A., Petrosyan, P., Clark, A.P., Liu, Z., Eggert, P., Pierce, J., Knowles, J.A., Ames, J., Kesselman, C., Toga, A.W., Potkin, S.G., Vawter, M.P., Macciardi, F., 2012. Next generation sequence analysis and computational genomics using graphical pipeline workflows. *Genes (Basel)* 3, 545–575.
- Troili, F., Cipollini, V., Moci, M., Morena, E., Palotai, M., Rinaldi, V., Romano, C., Ristori, G., Giubilei, F., Salvetti, M., Orzi, F., Guttman, C.R.G., Cavallari, M., 2020. Perivascular unit: this must be the place. The anatomical crossroad between the immune, vascular and nervous system. *Front. Neuroanat.* 14, 1–17.
- Tustison, N.J., Avants, B.B., Cook, P.A., Zheng, Y., Egan, A., Yushkevich, P.A., Gee, J.C., 2010. N4ITK: improved N3 bias correction. *IEEE Trans. Med. Imaging* 29, 1310–1320.
- Valdés Hernández, M. del C., Ballerini, L., Glatz, A., Muñoz Maniega, S., Gow, A.J., Bastin, M.E., Starr, J.M., Deary, I.J., Wardlaw, J.M., 2020. Perivascular spaces in the centrum semiovale at the beginning of the 8th decade of life: effect on cognition and associations with mineral deposition. *Brain Imaging Behav.* 14, 1865–1875.
- Wardlaw, J.M., Benveniste, H., Nedergaard, M., Zlokovic, E.F., Mestre, H., Lee, H., Doubal, F.N., Brown, R., Ramirez, J., Macintosh, B.J., Tannenbaum, A., Ballerini, L., Rungta, R.L., Boido, D., Sweeney, M., Montagne, A., Charpak, S., Joutel, A., Smith, K.J., Black, S.E., Hurvitz, Brain, H., Zlokovic, B.V., Mestre, H., Lee, H., Doubal, F.N., Brown, R., Ramirez, J., Macintosh, B.J., Tannenbaum, A., Ballerini, L., Rungta, R.L., Boido, D., Sweeney, M., Montagne, A., Charpak, S., Joutel, A., Smith, K.J., Black, S.E., 2020a. Perivascular spaces in the brain: anatomy,

- physiology, and contributions to pathology of brain diseases, nature reviews neurology. *Nat. Res.* 16, 137–153.
- Wardlaw, J.M., Benveniste, H., Nedergaard, M., Zlokovic, B.V., Mestre, H., Lee, H., Doubal, F.N., Brown, R., Ramirez, J., MacIntosh, B.J., 2020b. Perivascular spaces in the brain: anatomy, physiology and pathology. *Nat. Rev. Neurol.* 1–17.
- Waters, A.B., Mace, R.A., Sawyer, K.S., 2018. Identifying errors in Freesurfer automated skull stripping and the incremental utility of manual intervention.
- Wechsler, D., 1987. *Manual for the Wechsler Memory Scale-Revised*. TX Psychol. Corp., San Antonio.
- Weiner, M.W., Veitch, D.P., Aisen, P.S., Beckett, L.A., Cairns, N.J., Green, R.C., Harvey, D., Jack, C.R., Jagust, W., Morris, J.C., Petersen, R.C., Salazar, J., Saykin, A.J., Shaw, L.M., Toga, A.W., Trojanowski, J.Q., 2017. The Alzheimer's Disease Neuroimaging Initiative 3: continued innovation for clinical trial improvement. *Alzheimer's Dement.* 13, 561–571.
- Weller, R., Subash, M., Preston, S., Mazanti, I., Carare, R., 2008a. Perivascular drainage of amyloid- $\beta$  peptides from the brain and its failure in cerebral amyloid angiopathy and Alzheimer's disease. *Brain Pathol.* 18, 253–266.
- Weller, R.O., Subash, M., Preston, S.D., Mazanti, I., Carare, R.O., 2008b. SYMPOSIUM: Clearance of A $\beta$  from the brain in Alzheimer's disease: perivascular drainage of amyloid- $\beta$  peptides from the brain and its failure in cerebral amyloid angiopathy and Alzheimer's disease. *Brain Pathol.* 18, 253–266.
- Wiest-Daesslé, N., Prima, S., Coupé, P., Morrissey, S.P., Barillot, C., 2008. Rician noise removal by non-local means filtering for low signal-to-noise ratio MRI: applications to DT-MRI. *International Conference on Medical Image Computing and Computer-assisted Intervention*. Springer, Berlin, Heidelberg, pp. 171–179.
- Xu, Z., Xiao, N., Chen, Y., Huang, H., Marshall, C., Gao, J., Cai, Z., Wu, T., Hu, G., Xiao, M., 2015. Deletion of aquaporin-4 in APP/PS1 mice exacerbates brain A $\beta$  accumulation and memory deficits. *Mol. Neurodegener.* 10, 58.
- Zhang, X., Ding, L., Yang, L., Qin, W., Yuan, J., Li, S., Hu, W., 2016. Brain atrophy correlates with severe enlarged perivascular spaces in basal ganglia among lacunar stroke patients. *PLoS One* 11, 1–9.
- Zhu, Y.C., Dufouil, C., Soumaré, A., Mazoyer, B., Chabriat, H., Tzourio, C., 2010a. High degree of dilated Virchow-Robin spaces on MRI is associated with increased risk of dementia. *J. Alzheimer's Dis.* 22, 663–672.
- Zhu, Y.-C., Tzourio, C., Soumare, A., Mazoyer, B., Dufouil, C., Chabriat, H., 2010b. Severity of dilated Virchow-Robin spaces is associated with age, blood pressure, and MRI markers of small vessel disease: a population-based study. *Stroke* 41, 2483–2490.
- Zong, X., Park, S.H., Shen, D., Lin, W., 2016. Visualization of perivascular spaces in the human brain at 7T: sequence optimization and morphology characterization. *Neuroimage* 125, 895–902.